

# Environmental Science Advances

Accepted Manuscript

This article can be cited before page numbers have been issued, to do this please use: K. Sharma, A. Srivastava, S. Dutta, R. K. Sharma, R. Jain, P. Kumar, R. Singh, P. Yadav, V. K. Upadhyay, G. Kalot and S. Kurur, *Environ. Sci.: Adv.*, 2026, DOI: 10.1039/D6VA00059B.



This is an Accepted Manuscript, which has been through the Royal Society of Chemistry peer review process and has been accepted for publication.

Accepted Manuscripts are published online shortly after acceptance, before technical editing, formatting and proof reading. Using this free service, authors can make their results available to the community, in citable form, before we publish the edited article. We will replace this Accepted Manuscript with the edited and formatted Advance Article as soon as it is available.

You can find more information about Accepted Manuscripts in the [Information for Authors](#).

Please note that technical editing may introduce minor changes to the text and/or graphics, which may alter content. The journal's standard [Terms & Conditions](#) and the [Ethical guidelines](#) still apply. In no event shall the Royal Society of Chemistry be held responsible for any errors or omissions in this Accepted Manuscript or any consequences arising from the use of any information it contains.

## Environmental Significance

View Article Online  
DOI: 10.1039/D6VA00059B

The review focuses on the rational design of magnetic metal oxide@graphene oxide (MMO@GO) based nanocomposites, especially in context to their role in the sustainable photocatalytic degradation of a plethora of organic pollutants- including pharmaceuticals such as antimicrobials, antipyretics, antidiabetics etc, microplastics, dyes and pesticides. This work significantly aligns with various UN Sustainable Development Goals by promoting visible light driven photocatalysis, high reusability and minimum secondary waste generation.



## ARTICLE

**Towards Sustainable Photocatalytic Degradation of Organic Pollutants through Rational Design of Engineered Magnetically Retrievable Metal Oxide@Graphene Oxide Nanocomposites**Kirti <sup>a</sup>, Anju Srivastava <sup>a\*</sup>, Sriparna Dutta <sup>a\*</sup>, R. K. Sharma <sup>b</sup>, Reena Jain <sup>a</sup>, Prashant Kumar <sup>c</sup>, Ruchi Singh <sup>a</sup>, Priyanka <sup>a</sup>, Vipin Kumar Upadhyay <sup>d</sup>, Geetanshu <sup>a</sup> and Siddharth N Kurur <sup>e</sup>Received 00th January 20xx,  
Accepted 00th January 20xx

DOI: 10.1039/x0xx00000x

<sup>a</sup> Department of Chemistry, Hindu College, University of Delhi, Delhi-110007.<sup>b</sup> Green Chemistry Network Centre, Hindu College, University of Delhi, Delhi-110007.<sup>c</sup> Department of Chemistry, SRM University Delhi-NCR, Sonapat, Haryana 131029<sup>d</sup> Department of Chemistry, IIT Kanpur, Kanpur- 208016.<sup>e</sup> Department of Chemistry, University of Delhi, Delhi-110007.

Toxic pollutants in aqueous media cause great harm to both the environment and living beings thus; the remediation of such pollutants through the design and development of highly efficient and recyclable nanomaterials is pivotal. These nanoscale platforms enable superior adsorption and catalytic performance while minimizing energy input and secondary waste compared to conventional treatment technologies. Among the various nanomaterials investigated, magnetically retrievable graphene oxide nanocomposites have emerged as highly promising candidates for the remediation of a large array of pollutants, including heavy metals and organic contaminants such as dyes, pesticides, herbicides, and pharmaceuticals. The outstanding performance of such nanocomposites is attributed to their high specific surface area, which enables increased adsorption capacity, superior degradation efficiency, excellent stability, ease of magnetic separation, facile modification and functionalization,. Furthermore, recent studies have demonstrated that coupling semiconducting metal oxides with graphene oxide-based nanocomposites yields photoactive materials with tailored band gaps, capable of harnessing solar or visible light for photocatalytic degradation, thereby providing an affordable, efficient, and sustainable strategy for treating air and water contamination. This review examines the synthesis and functionalization of such nanomaterials, with particular emphasis on their photocatalytic pollutant removal mechanisms. By integrating mechanistic insights with application-oriented considerations, this work offers a cohesive framework for the rational design of sustainable, reusable, and efficient nanomaterials for environmental remediation and water purification. In doing so, it bridges fragmented research efforts, highlights future research directions, and provides actionable insights for translating laboratory innovations into real-world environmental remediation solutions.

processes lead to the contamination of our natural resources, including air, water, and soil. This has made air unbreathable, water undrinkable, and soil unfit for cultivation, leading to various diseases and environmental concerns such as cancer, asthma, heart and brain diseases, and global warming<sup>2,3</sup>. Organic pollutants in particular are one of the major causes of water and air pollution<sup>4,5</sup>. The World Health Organization (WHO) claims that even low concentrations of these persistent organic pollutants (POPs) can cause harmful health effects, such as a higher risk of cancer, compromised immune response, neurological effects, endocrine disruption, genotoxicity, and birth defects.

**1. Introduction**

Industrialization has played a pivotal role in the development of modern society by revolutionizing every aspect of human life. With the huge benefits and comforts industrialization has brought to our civilization, it is also the reason for the large-scale destruction of the earth's natural environment<sup>1</sup>. Pollutants such as heavy metals, organic pollutants, emerging micro-contaminants etc. and products released from industrial

<sup>a</sup> Department of Chemistry, Hindu College, University of Delhi, Delhi-110007.<sup>b</sup> Green Chemistry Network Centre, Hindu College, University of Delhi, Delhi-110007.<sup>c</sup> Department of Chemistry, SRM University Delhi-NCR, Sonapat, Haryana 131029<sup>d</sup> Department of Chemistry, IIT Kanpur, Kanpur- 208016.<sup>e</sup> Department of Chemistry, University of Delhi, Delhi-110007.

Therefore, targeting these POPs becomes an essential part of combating environmental pollution. With the current demand to combat these critical issues, numerous efforts have been made by researchers to capture and eliminate these pollutants from the environment using many techniques ranging from the simplest filtration-based methods to the most sophisticated methods involving artificial intelligence (AI)<sup>6-9</sup>. The current techniques are either not efficient enough or unaffordable or are not eco-friendly, making them unsuitable for a large-scale application<sup>9</sup>.

Photocatalysts have the ability to absorb light and produce reactive oxygen species (ROS) (Fig.1). ROS, including  $\bullet\text{OH}$  and  $\text{O}_2^{\bullet-}$ , cause deterioration of pollutants through a redox mechanism. The process employs light activated semiconductor catalysts to generate reactive oxygen species (ROS) that oxidize contaminants<sup>10</sup>. When the catalyst's surface is exposed to light with an energy equivalent to or greater than its band gap. Excitation of electrons occurs from the valence band to the conduction band generating holes in the valence band, resulting in the formation of electron hole ( $e^-/h^+$ ) pairs. ROS are produced when the electron-hole pairs interact with oxygenated species on the catalyst's surface, such as water and air.  $\text{O}_2^{\bullet-}$  is created by the electron through dissolved oxygen reduction, whereas  $\bullet\text{OH}$  and hydrogen gas are produced when water is oxidized by a hole. When  $\text{O}_2^{\bullet-}$  reacts with  $\text{H}_2\text{O}$ , it produces  $\text{H}_2\text{O}_2$  and increases the synthesis of  $\bullet\text{OH}$ . Although the degradation process achieves high efficiency in general, the efficiency of a specific nanocomposite is determined by several factors that can influence the formation of reactive radicals such as catalyst concentration, pharmaceutical concentration, dissolved oxygen levels, pH, water matrix, oxidant concentration, light source, and intensity<sup>11-16</sup>.

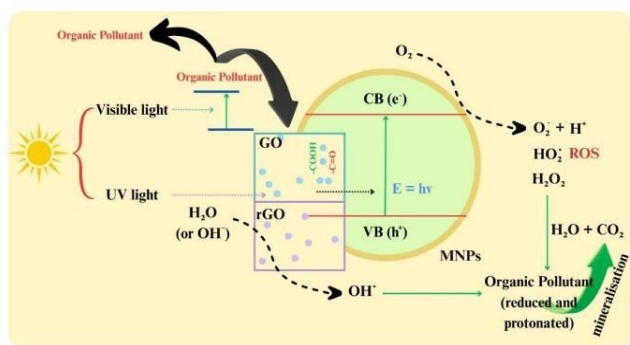


Fig. 1 Schematic representation of formation of ROS under UV and visible light irradiation on the photocatalyst

Metal oxides are considered promising candidates as photocatalysts owing to their low cost, high efficiency, simple synthesis routes, and sufficient availability<sup>17,18</sup>. However due to their wide band gap they require UV light to serve as a photocatalyst that, limits their usage<sup>19</sup>. When graphene oxide is coupled with metal oxides, it inhibits the recombination of photogenerated ( $e^-/h^+$ ) pairs enhancing the overall catalytic activity<sup>20</sup>. It also reduces the band gap of these metal oxides further enhancing their catalytic activity<sup>21,22</sup>. GO nanocomposites possess the appropriate band gap required to harness the solar energy or light for their photocatalytic activity, thereby making them an affordable, effective, and sustainable solution to treat air and water contamination<sup>23,24</sup>.

Graphene and graphene oxide (GO) based materials have been employed in diverse domains such as hydrogen storage, harmful gas removal, biomedical applications, etc. because of their unique physicochemical characteristics, including extensive active surface area, and high operational efficiency<sup>25,26</sup>. Researchers have reported that graphene oxide exhibits superior oxidizing properties compared to graphene because it carries oxygen rich functional groups such as hydroxyl ( $-\text{OH}$ ), carboxyl ( $-\text{COOH}$ ), and epoxy ( $-\text{COC}$ ) groups. Thus, its processing and synthesis become easier, making it more suitable for application. GO has been found to be a good candidate for the treatment of water however its high dispersibility, prevents easy separation from water after the absorption of pollutants<sup>27-29</sup>. To overcome this challenge, researchers have developed methods to magnetize GO by attaching magnetic moieties on its surface, enabling its easy separation from water using external magnetic field and allowing for reuse. Thus, magnetic graphene oxide-based nanocomposites are gaining popularity now a days in eliminating toxic pollutants like heavy metals and organic pollutants, including dyes, pesticides, herbicides, and pharmaceuticals owing to their unique physicochemical properties, such as strong magnetic and photocatalytic performances, large surface-active sites and surface area, high chemical stability, remarkable efficiency, good control of their morphological characteristics, and the ease with which they can be functionalized<sup>30-33</sup>.



[Type here]

## 2. Scope of Review

The review compiles recent advances in sustainable,



Fig.2 Different metal oxides which are popularly being used for making nanocomposites.

magnetically retrievable photocatalytic nanocomposites for the efficient degradation of hazardous organic pollutants in water, aligning with the United Nations Sustainable Development Goal 6 (Clean Water and Sanitation), which aims to ensure safe and clean water for all. The rational design of reusable metal oxide@graphene oxide photocatalysts promotes environmentally friendly and energy-efficient wastewater treatment technologies that support global water quality improvement objectives<sup>34-35</sup>. It seeks to present an extensive overview of magnetic metal oxide@graphene oxide (MMO@GO) based nanocomposites, emphasizing their synthesis, physicochemical properties, and their role in photocatalytic degradation of organic pollutants. A detailed overview of the fabrication methodologies implemented for producing MMO@GO hybrid nanomaterials, including coprecipitation, hydrothermal, and green synthesis techniques has been discussed. Insights into the utilization of MMO@GO and MMO@rGO (magnetic metal oxide@graphene oxide and magnetic metal oxide@reduced graphene oxide) nanocomposites in environmental remediation, particularly for the removal of organic pollutants including dyes, pesticides, pharmaceuticals and microplastics from aqueous solutions have been elaborated upon. A critical comparison of the magnetic metal oxide anchored graphene oxide nanocomposites has been made with the other reported photocatalysts taking into account all important parameters involved in assessing the quality of a catalyst. Lastly, current limitations and challenges in the field, along with proposed solutions and future research directions aimed at advancing the practical applications of MMO@GO based nanocomposites are addressed.

Although, until now, a number of review articles have been penned focusing on photocatalytic materials for the remediation of wastewater contaminated with organic pollutants, limited attention has been paid to the rational design, functionality, and potential of metal oxide-anchored

magnetically retrievable graphene oxide nanocomposites. It is expected that the rational design of such nanocomposites will provide a potential photocatalytic material for the efficient degradation of organic pollutants. With this background, this review article provides a comprehensive overview of the design strategies, mechanistic understanding, and recent developments in the design of MMO@GO nanocomposites for the efficient degradation of organic pollutants. It is expected that this compilation will help the scientific community in harnessing the potential of such nanocomposites in the future.

Lastly, current limitations and challenges in the field, along with proposed solutions and future research directions aimed at advancing the practical applications of MMO@GO based nanocomposites are addressed. Through this review we aim to provide a support to researchers and practitioners to explore and utilize the potential of MMO@GO based nanocomposites across scientific and industrial sectors.

## 3. Synthesis of Magnetic Metal Oxide@Graphene Oxide based Nanocomposites

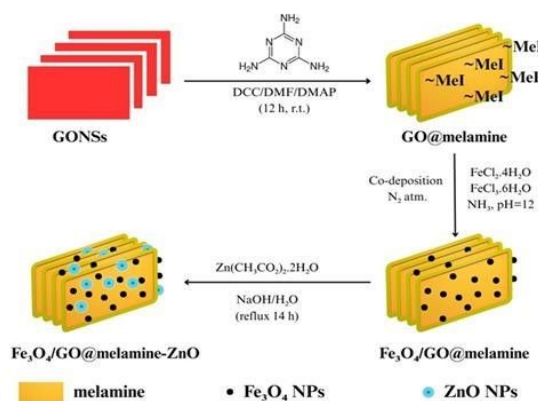


Fig.3 Schematic representation of  $\text{Fe}_3\text{O}_4@\text{GO}@\text{melamine-ZnO}$  nanocomposite

### 3.1 Synthesis of $\text{GO}@\text{ZnO}@\text{Fe}_3\text{O}_4$ and related nanocomposites

Metal oxides are utilized as components of photocatalytic systems due to their wide band-gaps and resistance to photo corrosion. Zinc oxide (ZnO) is a popular choice due to its very wide band-gap, low cost, high photocatalytic activity, and high chemical stability<sup>36</sup>. A key component among many of these hybrid systems is graphene oxide, generally synthesized through Hummer's method or its modified approaches. The classical Hummer's method was introduced in 1957 by William S Hummers, Jr. which offers a safer, faster alternative to the Staudenmaier Hofmann-Hamdi method involving a laborious and dangerous synthetic pathway due to the use of potassium chlorate in presence of concentrated  $\text{H}_2\text{SO}_4$  and  $\text{HNO}_3$ . Hummer's method<sup>37</sup> replaces these reagents with a water free



mixture of concentrated  $\text{H}_2\text{SO}_4$ , sodium nitrate and potassium permanganate to oxidize graphite. In contrast the modified Hummer's method described by Marcano *et al.*<sup>38</sup> eliminates the use of  $\text{NaNO}_3$  and employs a 9:1 mixture of  $\text{H}_2\text{SO}_4$  and  $\text{H}_3\text{PO}_4$ .

In 2020, Abbasi and co-workers<sup>39</sup> prepared  $\text{Fe}_3\text{O}_4@\text{ZnO}@\text{GO}$  nanocomposites and evaluated their photocatalytic performances towards the degradation of organic dye pollutants. Hydrothermal procedure was used to synthesise  $\text{Fe}_3\text{O}_4$  nanoparticles.  $\text{Fe}(\text{acac})_3$  was dispersed into ethylene glycol, followed by addition and mixing of  $\text{NH}_4\text{Ac}$ . The reaction mixture was heated at  $200^\circ\text{C}$  for 24 h before being cooled to room temperature. The synthesized compound was filtered, washed and dried at  $60^\circ\text{C}$  for 12 h. For the synthesis of  $\text{GO}@\text{Fe}_3\text{O}_4$ , a similar process was followed with the incorporation of GO followed by agitation using an ultrasound bath. The synthesized product was separated from the suspension using an external magnetic field. For synthesizing  $\text{GO}@\text{Fe}_3\text{O}_4@\text{ZnO}$  nanocomposites,  $\text{GO}@\text{Fe}_3\text{O}_4$  particles were dispersed in distilled water and agitated using an ultrasound bath, following which  $\text{ZnCl}_2$  was dissolved in the solution. The solution was heated to  $90^\circ\text{C}$  and NaOH solution was added dropwise under vigorous agitation. The powder obtained was separated, washed and dried at  $80^\circ\text{C}$  for 12 h and calcined at  $300^\circ\text{C}$ .

In parallel but with different intent, Eivazzadeh-Keihan *et al.* synthesized melamine functionalized  $\text{Fe}_3\text{O}_4@\text{ZnO}@\text{GO}$  nanocomposites and studied its use in organic catalysis and electrical capacitance. Graphene oxide nanosheets (GONS) were first activated with DCC and subsequently functionalized with melamine under ultrasonication (Fig.3). The resulting mixture was stirred at room temperature, centrifuged, and washed with ethanol. Next, a solution of iron chloride salts in deionized water was combined with the melamine-functionalized GONS. Afterthat,  $\text{Fe}_3\text{O}_4$  nanoparticles were synthesized and intercalated through an in-situ codeposition process carried out at a pH 12 under neutral atmospheric conditions. The obtained  $\text{Fe}_3\text{O}_4@\text{GO}@\text{melamine}$  nanoparticles were dispersed in deionized water, followed by the addition of zinc acetate and sodium hydroxide, and the mixture was stirred

for 1 h. The mixture was then subjected to vigorous stirring under reflux for 14 h. Finally, the synthesized nanocomposites were isolated using an external magnet, thoroughly washed, and dried at  $60^\circ\text{C}$ <sup>40</sup>.

Using magnesium ferrite as magnetic material, Bateni and coworkers<sup>41</sup> synthesized pectin/ $\text{GO}@\text{MgFe}_2\text{O}_4@\text{ZnO}$  nanocomposites to study the photocatalytic degradation of

aqueous solution of diclofenac. GO nanosheets were prepared using modified Hummer's method, while ZnO nanoparticles were synthesized by mixing aqueous solutions of NaOH and zinc nitrate, and refluxing at  $90^\circ\text{C}$ . Aqueous solutions of iron nitrate and magnesium nitrate were mixed and the synthesized ZnO nanoparticles were immersed with constant stirring. The resulting mixture was added slowly to NaOH solution, following which it was sealed at  $90^\circ\text{C}$ . Once cooled, the product was washed, centrifuged and dried at  $80^\circ\text{C}$  and then calcined at  $500^\circ\text{C}$ . Pectin@GO nanocomposite was synthesized with the help of DMAP and DCC as catalysts followed by addition of  $\text{ZnO}@\text{MgFe}_2\text{O}_4$  nanoparticles and stirring for 48h under ultrasonication. Centrifugation of the suspension and subsequent washing and drying yielded the required photocatalyst. Extending the applicability towards biomedical technology Salimi *et al.* synthesized  $\text{Fe}_3\text{O}_4@\text{ZnO}@\text{GO}$  nanocomposites for drug delivery applications. Hummer's method was used to synthesize graphene oxide. Magnetic ( $\text{Fe}_3\text{O}_4$ ) nanoparticles were synthesized *via* thermal treatment by mixing iron(II) nitrate and iron(III) nitrate in a solution with Polyvinylpyrrolidone(PVP). To synthesize  $\text{Fe}_3\text{O}_4@\text{ZnO}$  nanocrystals, iron oxide nanoparticles and zinc nitrate were mixed in the aquatic environment before synthesizing  $\text{Fe}_3\text{O}_4@\text{ZnO}@\text{GO}$  nanocomposites<sup>42</sup>.

### 3.2 Synthesis of $\text{GO}@\text{TiO}_2@\text{Fe}_3\text{O}_4$ and related nanocomposites

$\text{TiO}_2$  is abundant, non-toxic, environmentally benign, which has made it a widely studied material for environmental applications<sup>43,44</sup>. Over the past decade numerous  $\text{TiO}_2@\text{GO}@\text{magnetic}$  hybrid nano composites have been engineered to improve its catalytic properties. Cao *et al.* reported one of the earlier advancements in the field with the development of magnetically separable graphene- $\text{TiO}_2$  ( $\text{MGTiO}_2$ ) hybrid photocatalyst *via* a one-step method<sup>45,46</sup>. A modified Hummer's method was used to synthesized graphene oxide (GO) while a co-precipitation method was used to synthesized  $\text{Fe}_3\text{O}_4$  nanoparticles. The two solutions were mixed in a 1:1 weight ratio under continuous stirring for 1h and resulted in the formation of MGO composite. Subsequently the titania coated MGO composites were synthesized through a solvothermal approach using tetrabutyl titanate. The crystalline structure of the obtained samples was characterized by XRD while the band gaps of MGO- $\text{TiO}_2$  with  $\text{TiO}_2$  loadings of 0.5%, 1%, 3%, 5% were reported to be 3.15, 3.14, 3.11 and 3.06 eV, respectively.

Building on this concept Li *et al.* synthesized  $\text{TiO}_2@\text{graphene}@\text{Fe}_3\text{O}_4$  nanocomposites<sup>47-49</sup>. GO was synthesized *via* Hummer's method while Anatase  $\text{TiO}_2$  was



[Type here]

prepared using hydrolysis and hydrothermal treatment of  $\text{Ti}(\text{BuO})_4$ , and both were incorporated to form  $\text{TiO}_2@\text{GO}$ . In it, acid-resistant  $\text{Fe}_3\text{O}_4$  nanoparticles were introduced to mitigate  $\text{Fe}(\text{II})$  leaching.  $\text{TiO}_2$  is mixed with potassium hydroxide ( $\text{KOH}$ ) and potassium nitrate ( $\text{KNO}_3$ ), followed by  $\text{FeSO}_4$  under nitrogen purging. The mixture underwent hydrothermal treatment at  $90^\circ\text{C}$ , resulting in the formation of  $\text{TiO}_2@\text{graphene}@\text{Fe}_3\text{O}_4$ .

In the same year, Ghosh *et al.* engineered  $\text{TiO}_2@\text{CoFe}_2\text{O}_4@\text{rGO}$  nanocomposites<sup>50</sup> *via* a non-hydrothermal, water-based route. The method avoids the use of high-pressure autoclaves and organic solvents.  $\text{CoFe}_2\text{O}_4$  nanoparticles were prepared using an EFT assisted method, while incorporation of  $\text{TiO}_2$  occurred *via* a surfactant-assisted sol-gel process. GO was synthesized by employing Hummer's method and was reduced to rGO using hydrazine.  $\text{TiO}_2@\text{CoFe}_2\text{O}_4$  with GO dispersed were refluxed followed by chemical reduction and drying, yielded the final

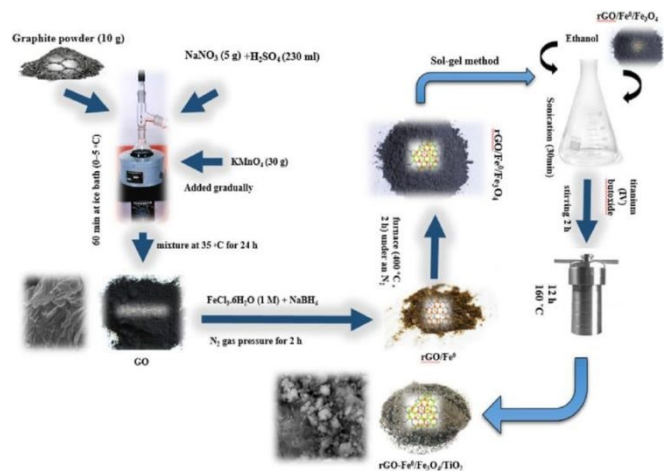


Fig.4 Schematic representation of the synthesis of rGO, rGO@Fe<sup>0</sup>, rGO@Fe<sup>0</sup>@Fe<sub>3</sub>O<sub>4</sub>, and rGO@Fe<sup>0</sup>@Fe<sub>3</sub>O<sub>4</sub>@TiO<sub>2</sub>. Reproduced from ref.51 with permission from Elsevier, copyright 2023

nanocomposites with a band gap of 2.22 eV and strong magnetic properties ( $M_s$ : 14.5 emu/g).

Continuing advancement in multifunctional photocatalytic systems, Qilong Li and co-workers synthesized  $\text{TiO}_2\text{-GO-Fe}_3\text{O}_4$  nanocomposites<sup>51</sup> through a multi-step fabrication approach with enhanced photo-Fenton catalysis and magnetic recovery. GO was prepared *via* Hummer's method and incorporated  $\text{TiO}_2$  through hydrothermal treatment at  $120^\circ\text{C}$  while the incorporation of  $\text{Fe}_3\text{O}_4$  was achieved by mixing of  $\text{Fe}(\text{NO}_3)_3\cdot 9\text{H}_2\text{O}$  in the former  $\text{GO-TiO}_2$  solution followed by ultrasonic treatment, drying, and alkaline treatment at  $180^\circ\text{C}$ . Reduction with ethylene glycol converted  $\text{Fe}(\text{OH})_3$  formed due to alkaline treatment to  $\text{Fe}_3\text{O}_4$ ; subsequently the composite was vacuum dried. The design improves charge separation, photocatalytic efficiency and magnetic separability.

In search of better synthesis approaches, in recent years further improvements have been made. Jamal *et al.* synthesized  $\text{rGO}@\text{FeO}@\text{Fe}_3\text{O}_4@\text{TiO}_2$  nanocomposites<sup>52</sup> wherein rGO were prepared *via* a modified Hummer's method by oxidizing

graphite powder using sodium nitrate and potassium permanganate in sulphuric acid followed by reduction using ascorbic acid. (Fig.4) Iron species were incorporated using sodium borohydride reduction and  $\text{TiO}_2$  was deposited through sol gel and hydrothermal treatment.

Similarly, Bala *et al.* synthesized  $\text{Cu}_2\text{O}@\text{CuO}$ -decorated  $\text{TiO}_2@\text{GO}$  nanocomposites<sup>53-55</sup> *via* a liquid impregnation method, ensuring uniform copper dispersion. GO was synthesized by a modified Hummer's method. The synthesis involves the treatment of  $\text{TiO}_2$  with copper(II) nitrate, followed by calcination at  $450^\circ\text{C}$  in argon and subsequent reduction at  $280^\circ\text{C}$  in  $\text{H}_2/\text{argon}$ . The resulting  $\text{Cu}_2\text{O}/\text{CuO-TiO}_2$  were dried with GO in a ratio of 10:1. The content of copper was varied (1-3%) and all the variants resulted in a decreased PL (photoluminescence) intensity indicating an effective charge carrier separation.

Gupta *et al.*<sup>56-57</sup> reported the synthesis of  $\text{CoFe}_2\text{O}_4@\text{TiO}_2/\text{rGO}$  nanocomposites.  $\text{CoFe}_2\text{O}_4$  nanoparticles were prepared using a co-precipitation method followed by incorporation of pre-calcined  $\text{TiO}_2$  under alkaline conditions at  $90^\circ\text{C}$ . The rGO were prepared using a modified Hummer's method and the  $\text{CoFe}_2\text{O}_4@\text{TiO}_2/\text{rGO}$  composite was formed by addition of stoichiometric ratio of  $\text{CoFe}_2\text{O}_4@\text{TiO}_2$  into a ultrasonicated rGO suspension in water followed by refluxing the suspension at  $95^\circ\text{C}$  for 2 h (Fig.5).

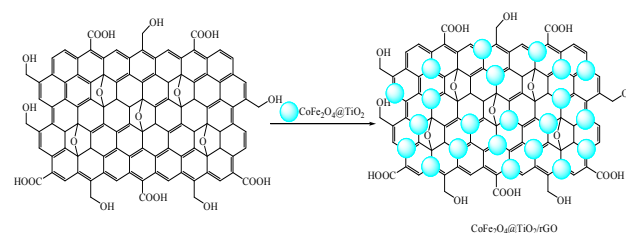


Fig. 5 rGO@TiO<sub>2</sub>@CoFe<sub>2</sub>O<sub>4</sub> nanocomposite synthesis

### 3.3 MnO<sub>2</sub>@Fe<sub>3</sub>O<sub>4</sub>@rGO and related nanocomposites

Manganese dioxide ( $\text{MnO}_2$ ) has garnered significant research interest and attention owing to its unique physicochemical characteristics, as well as its extensive applications in supercapacitors<sup>58</sup>, batteries<sup>59</sup>, microwave adsorption<sup>60</sup>, visible lightdriven catalysis<sup>61</sup>, molecular sieves<sup>62</sup>, and water purification<sup>63</sup>. Nevertheless, the structural instability, inadequate electroconductivity and difficulty in separation, considerably limit its practical applications<sup>64</sup>. To enhance its performance further, it is essential to integrate other materials with  $\text{MnO}_2$ . The incorporation of  $\text{Fe}_3\text{O}_4$  and  $\text{GO}@\text{rGO}$  can improve the properties of  $\text{MnO}_2$ , as  $\text{Fe}_3\text{O}_4$  demonstrates commendable electronic conductivity<sup>65</sup>. Additionally, as part of a composite,  $\text{Fe}_3\text{O}_4$  facilitates the recycling of multifunctional nanoparticles and enhances their stability<sup>61</sup>.  $\text{GO}@\text{rGO}$  provides



an extremely large surface area strong mechanical stability, and exceptional electrical conductivity.

The general scheme for the synthesis of  $\text{MnO}_2@Fe_3O_4@GO$  and  $\text{MnO}_2@Fe_3O_4@rGO$  nanocomposites as proposed by Yan Liu *et al.*<sup>66</sup> involves the preparation of GO by modified Hummer's method from natural flake like graphite. This is followed by the standard one-pot solvothermal method for the synthesis of  $Fe_3O_4@graphene$  oxide nanocomposite. Finally,  $MnO_2$  is coated with  $Fe_3O_4@GO$  by simple immersion into  $KMnO_4$  solution whose pH is controlled using HCl at 80°C for 3h. The research indicated that  $MnO_2@Fe_3O_4@GO$  exhibits a remarkable maximum adsorption capacity in both acidic and nearly neutral environments. The desorption results demonstrated that the adsorption capacity could persist at 76% after five cycles of use, suggesting that the  $MnO_2@Fe_3O_4@GO$  nanocomposite is a promising candidate for Cr(VI) adsorption.

A similar approach was used by Lichao Tan *et al.* in 2015<sup>67</sup> and Jing Li *et al.* in 2017<sup>68</sup> for the synthesis of  $MnO_2@Fe_3O_4@rGO$  nanocomposites. A three-dimensional (3D) hierarchical  $MnO_2$  shell was observed, with a  $Fe_3O_4@MnO_2$  core-shell structure coated by rGO layers. An examination of their electrical properties demonstrated that the effectiveness of the connection between  $Fe_3O_4@MnO_2$  particles and graphene layers significantly affects the electrocapacitive performance of the  $Fe_3O_4@MnO_2@rGO$  composite<sup>66</sup>. Moreover, the  $MnO_2@Fe_3O_4@rGO$  composite was found to be effective as an adsorbent for the sorption of uranium(VI)<sup>67</sup>.

#### 3.4 Synthesis of $V_2O_5@Fe_3O_4@rGO$ and related nanocomposites

In recent decades, vanadium pentoxide ( $V_2O_5$ ) has garnered significant interest among transition metal oxides due to its remarkable characteristics when combined with various supports for a range of applications<sup>69</sup>.  $V_2O_5$  acts as a semiconductor metal oxide catalyst with a low band gap energy of 2.2 eV, which readily facilitates electron-hole recombination when exposed to light. Consequently, hybrid systems composing of  $V_2O_5$  nanoparticles with reduced graphene oxide (rGO) sheets have demonstrated enhanced photocatalytic activity<sup>70</sup>. The incorporation of graphene sheets mitigates the premature recombination of electron-hole pairs, thus rendering them more accessible for photocatalytic processes. Additionally,  $Fe_3O_4$  enhances conductivity and imparts magnetic properties, which contribute to its effective recovery.

Synthesis of  $Fe_3O_4@V_2O_5@rGO$  nanocomposite by Purna K. Boruah *et al.*<sup>71</sup> describes an ex-situ method where  $Fe_3O_4$  NPs can be deposited on the surface of  $V_2O_5@rGO$  nanocomposite through chemical co-precipitation. The narrow band gap and

distinct band gap energies of  $Fe_3O_4$  and  $V_2O_5$  demonstrated its suitability for visible light absorption. DOI: 10.1039/D6VA00059B

Fatemeh Jafari *et al.*<sup>72</sup> proposed a different method for the synthesis of  $Fe_3O_4@V_2O_5@rGO$  nanocomposite involving the dissolution of  $Fe_3O_4@GO$  powder in ethylene glycol with a pH of 11-12 controlled by ammonia solution (25%). This is followed by the addition of  $NH_4VO_3$ , stirring and heating, autoclaving, washing, drying and finally annealing to form the composite. A similar strategy can be employed to synthesize  $Fe_3O_4@V_2O_5@GO$  nanocomposites. The results indicate that the graphene oxide substrate is effectively decorated using  $Fe_3O_4$  and  $V_2O_5$  nanoparticles and converted to reduced graphene oxide. Photoluminescence (PL) and diffuse reflectance spectroscopy (DRS) findings suggest, the incorporation of both  $V_2O_5$  and  $Fe_3O_4$  nanoparticles onto the reduced graphene oxide (rGO) nanosheets in the  $V_2O_5@Fe_3O_4@rGO$  composite significantly diminished the intensity and optical band gap energy, leading to enhanced charge transfer and reduced recombination of electron-hole pairs. The  $V_2O_5@Fe_3O_4@rGO$  composite demonstrates superior oxygen evolution activity, achieving an overpotential of 458 mV and a Tafel slope of 132 mV dec<sup>-1</sup> in LSV, outperforming rGO,  $Fe_3O_4$ ,  $V_2O_5$ ,  $Fe_3O_4@rGO$ , and  $V_2O_5@rGO$ .

#### 3.5 Synthesis of $ZrO_2@Fe_3O_4@rGO$ and related nanocomposites

Zirconium oxide nanoparticles ( $ZrO_2$  NPs), exhibit exceptional chemical and physical properties that render them highly versatile for various applications, such as fuel cells, gas sensors, optoelectronics, catalysts, and materials resistant to corrosion<sup>73-77</sup>. Owing to its large surface area and the presence of numerous oxygen vacancies, zirconium oxide is regarded as a promising candidate for photocatalytic applications within academic and scientific research<sup>78-81</sup>. As an adsorbent, zirconium enhances the adsorption process. The creation of  $ZrO_2$  nanocomposites with  $Fe_3O_4$  and GO/rGO results in improved characteristics and facilitates the recovery of the composite due to its magnetic properties.

In 2018, Nagi M. El-Shafai *et al.*<sup>82</sup> described a simple method for the synthesis of  $ZrO_2@Fe_3O_4@rGO$  in which GO sheets are dispersed in water and a solution containing  $ZrOCl_2 \cdot 8H_2O$ ,  $FeCl_2 \cdot H_2O$  and  $FeCl_3 \cdot 6H_2O$  is added followed by addition of hot ethanolic KOH solution drop wise with continuous stirring. The reaction mixture is centrifuged, washed and vacuum dried to obtain the  $ZrO_2@Fe_3O_4@rGO$  nanocomposite. The synthesized  $GO-Fe_3O_4@ZrO_2$  nanocomposite exhibited an energy band gap of 3.20 eV, as determined by optical absorption measurements, which was lower than that of GO and  $GO-Fe_3O_4$ . Additionally,



[Type here]

the composite demonstrated enhanced adsorption capacity and photocatalytic activity.

A recent research by Ali Fadhil Ismail *et al.*<sup>83</sup> showed that  $ZrO_2@Fe_3O_4@rGO$  nanocomposite can be prepared by adding a calculated amount of  $ZrO_2$  to aq. dispersion of  $Fe_3O_4@rGO$  and vigorously shaking the mixture for 1 h. This method can be used to synthesize  $ZrO_2@Fe_3O_4@rGO$  as well. Utilizing X-ray diffraction (XRD), field emission scanning electron microscopy (FESEM), and energy dispersive X-ray (EDX) analysis, it was confirmed that an amorphous phase was present, as evidenced by the strong peak positions at various lattice planes. The irregular shapes of the particles showed signs of aggregation.

### 3.6 Other Significant Contributions

In this section, synthesis of graphene oxide and  $Fe_3O_4$  based nanocomposites which are less explored among the scientific community have been discussed. Cu based nanocomposites have been shown to be effective catalysts for the oxidation of n-hexane<sup>84</sup> and have also been employed in high performance super-capacitor applications<sup>85</sup>. They are also being studied for the photo-catalytic effectiveness under the visible light for the degradation of organic pollutant<sup>86-88</sup>. There are few reports in the literature regarding the synthesis of Cu-based magnetic metal oxide@GO nanocomposites which include  $CuO@Fe_3O_4@GO$  and  $CuS_2@Fe_3O_4@GO$  nanocomposites. A general approach to synthesize such composites as highlighted by Yachana Jain *et al.*<sup>89</sup> and Negin Nasseh *et al.*<sup>90</sup>, includes the synthesis of GO using Hummer's method followed by sonochemical attachment of  $Fe_3O_4$  and  $CuS_2$  or  $CuO$  nanoparticles on its surface (Fig.6).

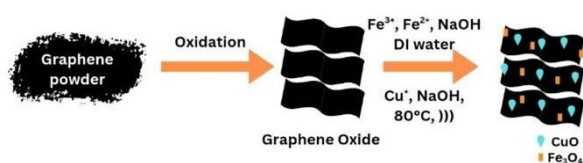


Fig.6 Schematic representation of synthesis of  $GO-Fe_3O_4@CuO$  nanocomposites.

In the former, the Ms value of the synthesized nanocomposite was found to be lower than that of pure magnetite. Nevertheless, the magnetization remained sufficiently high, allowing for the effective removal of the catalyst from the reaction mixture. The XRD analysis of the synthesized catalyst revealed that the crystal structure of the  $Fe_3O_4$  core remained unchanged during its immobilization on the surface of graphene oxide (GO). The absence of copper signals in the XRD pattern suggested that the Cu species are highly dispersed. Furthermore, no characteristic peaks of other impurities were identified. The composite demonstrated superior thermal

stability compared to GO. TEM images clearly revealed that  $Fe_3O_4$  and  $CuO$  nanoparticles had successfully integrated onto multilayer graphene oxide sheets. The synthesized catalyst exhibited remarkable catalytic activity and could be recycled up to 8 times. In the latter, the average size of  $CuS$  nanoparticles in the CS88F6G6 composite was reduced in comparison to its pure form. Additionally, the  $Fe_2O_3$  nanoparticles possessed fine pores within their structure, which function as a template to inhibit the growth of  $CuS$  nanoparticles, thereby increasing the surface area for photocatalytic activity. The spherical CFS nanoparticles were unevenly dispersed on surface of the smooth GO sheets. The CS88F6G6 nanocomposite exhibited superparamagnetic behaviour when subjected to an external magnetic field, allowing for easy recovery. Moreover, the nanocomposite showed a strong absorption in the 400–700 nm range, making it highly suitable for visible-light-driven photocatalysis.

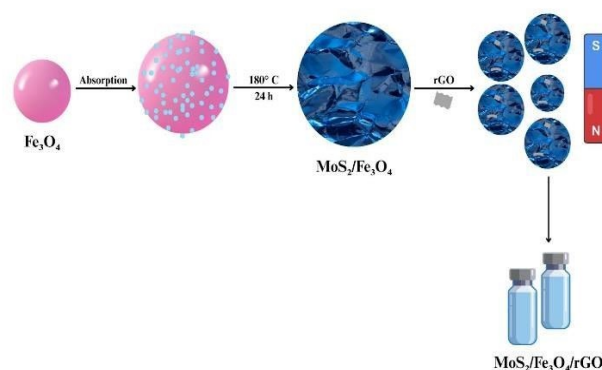


Fig. 7 Proposed mechanism for the formation of  $MoS_2@Fe_3O_4@rGO$  nanoparticles

Molybdenum sulfide ( $MoS_2$ ) is an n-type semiconductor<sup>91</sup> that has attracted considerable attention in the fields of photocatalysis<sup>92</sup>, sensors<sup>93</sup>, electrochemistry<sup>94</sup>, supercapacitors<sup>95</sup>, and drug delivery<sup>96</sup> owing to its natural abundance, well-developed crystalline structure, low production cost, favourable electrical conductivity, and large specific surface area. Moreover, the combination of  $MoS_2$  with  $Fe_3O_4$  and GO addresses the limitations of individual materials: such as the high density of  $Fe_3O_4$ <sup>97</sup>, issues with dispersion, and the tendency for two-dimensional GO and  $MoS_2$  to stack, thereby enhancing wave absorption performance<sup>98</sup> and safeguarding the magnetic metals<sup>99</sup>. Many researches have focused on the synthesis of  $MoS_2@Fe_3O_4@rGO$  with only the recent paving the pathway for the direct synthesis of  $Fe_3O_4@rGO@MoS_2$  and  $Fe_3O_4@rGO@Ag@MoS_2$  nanocomposites. (Fig.7)

In 2018, Dongzhao Mu *et al.*<sup>100</sup> synthesized  $MoS_2@Fe_3O_4@rGO$  nanocomposites using a simple procedure by dispersing the



monodispersed  $\text{Fe}_3\text{O}_4$  nanoparticles in distilled water under ultrasonic radiation followed by the slow addition of  $\text{Na}_2\text{MoO}_4$  and L-Cysteine under mechanical stirring at room temperature.

This was followed by the dropwise addition of GO suspension with continuous stirring then autoclaving the reaction mixture at  $180^\circ\text{C}$  for 24 h. The physicochemical properties of the prepared nanocomposite are displayed in Table 1.

Table 1: The corresponding physicochemical properties of  $\text{MoS}_2$ ,  $\text{MoS}_2@\text{Fe}_3\text{O}_4$  and  $\text{MoS}_2@\text{Fe}_3\text{O}_4@\text{rGO}^{100}$

Sample	Average Crystal Size [nm] (Standard deviation) <sup>1</sup>	$S_{\text{BET}}$ [ $\text{m}^2 \text{g}^{-1}$ ]	Pore [nm] ( $\text{cm}^3 \text{g}^{-1}$ )
$\text{MoS}_2$	18.22	8.16	0.04
$\text{MoS}_2@\text{Fe}_3\text{O}_4$	21.32	22.59	0.12
$\text{MoS}_2@\text{Fe}_3\text{O}_4@\text{rGO}$	10.27	72.23	0.185

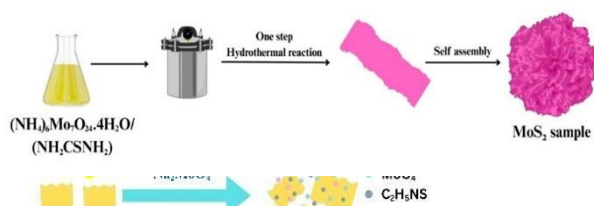


Fig. 9 The process of preparing  $\text{MoS}_2$  by one-step hydrothermal reaction

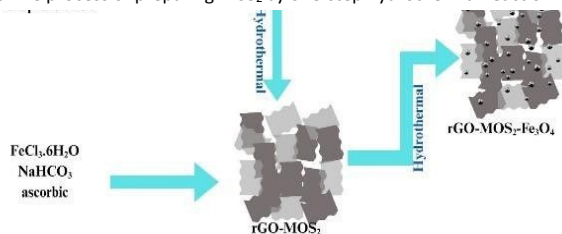


Fig. 8 Schematic illustration for the preparation of  $\text{rGO-MoS}_2\text{-Fe}_3\text{O}_4$  nanocomposite

A similar procedure was followed by Somayeh Tajik *et al.*<sup>101</sup> for the synthesis of  $\text{MoS}_2@\text{Fe}_3\text{O}_4@\text{rGO}$  nanocomposites (Fig. 8-9).

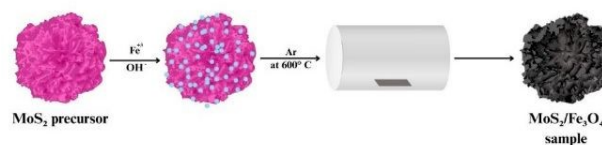


Fig.10 The preparation process of  $\text{MoS}_2@\text{Fe}_3\text{O}_4$  Composites

A different two-step hydrothermal method was proposed by Xiao Ding *et al.*<sup>102</sup> for the preparation of  $\text{rGO-MoS}_2$  composite:

The preparation included the synthesis of GO nanoparticles using the modified Hummer's method followed by ultrasonic dispersion and slow addition of aq. sodium molybdate and

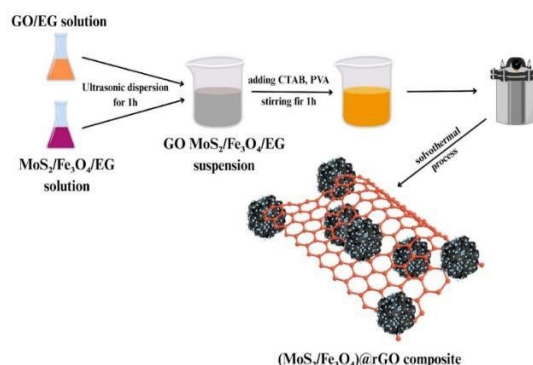


Fig. 11 Synthesis of porous  $\text{MoS}_2@\text{Fe}_3\text{O}_4@\text{rGO}$  composites thioacetamide; autoclaving the mixture at  $220^\circ\text{C}$  for 24 h and separating the product through centrifugation. The second step included the dispersion of  $\text{FeCl}_3\cdot 6\text{H}_2\text{O}$ ,  $\text{NaHCO}_3$ , ascorbic acid and  $\text{rGO}@\text{MoS}_2$  composite in water through ultra-sonication followed by autoclaving at  $180^\circ\text{C}$  for 18h. The  $\text{MoS}_2@\text{Fe}_3\text{O}_4@\text{rGO}$  composite was obtained by cooling, washing and then freeze-drying the ppt. overnight. The synthesized nanocomposite featured a three-dimensional architectural structure and demonstrated remarkable microwave absorption capabilities despite its minimal thickness. The lowest reflection loss (RL) recorded was 47.67 dB at a frequency of 17.44 GHz with a thickness of 1.5 mm. Additionally, maximum effective absorption bandwidth (RL B10



[Type here]

dB) achieved was 4.72 GHz when the thickness was increased to 1.7 mm.

Zhenjun Wang<sup>103</sup> synthesized 3D flower-like MoS<sub>2</sub>@Fe<sub>3</sub>O<sub>4</sub>@rGO composites using a three-step process involving the synthesis of MoS<sub>2</sub> through a one-step hydrothermal method, followed by preparation of MoS<sub>2</sub>@Fe<sub>3</sub>O<sub>4</sub> as shown in (Fig. 10).

This was followed by the preparation of MoS<sub>2</sub>@Fe<sub>3</sub>O<sub>4</sub>@rGO via ultrasonic dispersion of GO/EG solution and MoS<sub>2</sub>@Fe<sub>3</sub>O<sub>4</sub>@EG(ethylene glycol) solution, resulting in GO@MoS<sub>2</sub>@Fe<sub>3</sub>O<sub>4</sub> suspension. The final composite was then obtained through a solvothermal process (Fig.10). The core-shell composite MoS<sub>2</sub>@Fe<sub>3</sub>O<sub>4</sub>@rGO demonstrated a minimum reflection loss (RL) of -64.05 dB at a frequency of 1.83 mm, along with an effective absorption bandwidth (RL < -10 dB) of 7.34 GHz at 2.5 mm (spanning from 10.66 to 18 GHz), which was significantly greater than that of pure MoS<sub>2</sub> and MoS<sub>2</sub>@Fe<sub>3</sub>O<sub>4</sub> microspheres.

Latest research by Shilpa R Amonkar and Sudhir Cherukulappurath<sup>104</sup> shows that MoS<sub>2</sub>@Fe<sub>3</sub>O<sub>4</sub>@GO nanocomposites can be easily synthesized using the following approach. In addition to this Fe<sub>3</sub>O<sub>4</sub>@GO@Ag@MoS<sub>2</sub> can also be synthesized using the same procedure employing Fe<sub>3</sub>O<sub>4</sub>@GO@Ag as a substrate. The SEM image of Fe<sub>3</sub>O<sub>4</sub>@MoS<sub>2</sub> demonstrated that the hybrid composite is composed of both Fe<sub>3</sub>O<sub>4</sub> nanoparticle clusters and flower-like MoS<sub>2</sub> microspheres. It was noted that the Fe<sub>3</sub>O<sub>4</sub> clusters were enveloped by the flower-like MoS<sub>2</sub> microspheres (Fig.11)

As evident from the above discussions, to summarize the synthesis of magnetically retrievable metal oxide@Graphene Oxide nanocomposites involves the preparation of three different components - the magnetic material, the metal oxide and Graphene Oxide (GO)-and their integration to produce the nanocomposites.

The nanoparticles of various magnetic materials such as Fe<sub>3</sub>O<sub>4</sub>, CoFe<sub>2</sub>O<sub>4</sub>, and CuFe<sub>2</sub>O<sub>4</sub> are prepared using common methods of nanoparticle synthesis including hydrothermal, solvothermal, co-precipitation and sol-gel methods. The photocatalytic metal oxides such as ZnO, TiO<sub>2</sub>, and CuO are synthesized using hydro- or solvothermal methods, while GO is synthesized using the Hummers or Modified Hummers method. The most commonly used method for the synthesis of nanocomposites first involves the preparation of GO/magnetic material composite, followed by the dispersion of the synthesized metal oxide<sup>105</sup>. However, other methods of synthesis have also been developed by altering the order in which the different components are introduced, as well as through the *in situ* synthesis of nanoparticles in the reaction medium<sup>106-107</sup>.

#### 4. Photocatalytic Degradation of Wastewater Pollutants

This section explains the role of magnetic metal oxide@grapheneoxide based nanocomposites in photocatalytic degradation of organic pollutants generally found in wastewater.

##### 4.1 Pharmaceuticals

Pharmaceuticals represent a category of both synthetic and natural chemicals that possess bioactive properties, specifically formulated and produced to provide therapeutic benefits against illnesses or to prevent the onset and transmission of diseases in humans and animals. These substances can be found in the forms of over-the-counter medications, prescription drugs, or veterinary treatments<sup>108</sup>. The increasing prevalence of these compounds is observed yearly around the globe, driven by the emergence of new illnesses and the introduction of novel pharmaceuticals aimed at treating these conditions. Recent data from IQVIA reveals that the worldwide consumption of medicines has surged by 14% over the last five years and is anticipated to rise by an additional 12% by 2028, reaching an annual total of 3.8 trillion defined daily doses<sup>109</sup>. However, the extensive use of pharmaceuticals in everyday life have led to the emergence of contaminants, potentially harming both human health and aquatic ecosystems<sup>110-112</sup>. Globally over 3000 chemical substances, with concentrations varying from ng/L to µg/L, including pharmaceuticals, have been detected in wastewater, surface water, soil, groundwater, and drinking water<sup>113-115</sup>. Pharmaceutical compounds can enter the environment through direct discharges from drug manufacturing, excretion by patients and animals, aquaculture, and the inappropriate disposal of unused or expired medications, resulting in environmental contamination (UNEP). The existence of these pharmaceutical pollutants poses serious risks, including cancers, organ damage, congenital abnormalities, reproductive issues, endocrine disturbances, and a range of toxic effects, from mild to severe, in the global population. The toxic effects of these chemicals have also been observed in mammals and other living beings, and the overall ecosystem<sup>116</sup>. Furthermore, antibiotic-resistant bacteria can emerge and antibiotic-resistant gene may spread among humans and other organisms due to the accumulation of antibiotic medications in water sources<sup>117</sup>.

Heterogeneous photocatalysis has been shown by many studies to be an efficient, eco-friendly and economical method for the degradation of pharmaceutical contaminants<sup>118,119</sup>. The various magnetic metal oxide@GO photocatalytic agents that have been reported for the breakdown of different types of pharmaceutical agents have been covered in the following subsections.

View Article Online  
DOI: 10.1039/D6VA00059B



#### 4.1.1 Antimicrobials

Antimicrobials are chemotherapeutic substances that encompass a widely utilized category of agents, including antibiotics, antivirals, antifungals, and antiparasitics, aimed at preventing and treating infections in humans, aquaculture, livestock, and crops due to various pathogenic bacteria, viruses, fungi, and more. They were designed to reduce mortality rates and enhance the immune response in both humans and animals. However, only 30% of the developed antibiotics are currently employed in combating diseases, while the remaining 70% are improperly released into the environment without undergoing metabolism. Majority of these antimicrobials in the environment are poorly metabolised which allows them to persist there and lets them enter the food chain. These are ingested by both humans and animals; consequently, it facilitates the emergence and spread of antibiotic-resistant bacteria and antibiotic resistance genes<sup>111, 120</sup>. Thus, there has been a primary focus on their removal from aqueous environments through a photocatalytic approach.

A magnetically recyclable  $\text{CuFe}_2\text{O}_4@\text{rGO}$  nanocomposite with varying concentrations of graphene oxide was synthesized using the hydrothermal method by Aruljothi *et al.*<sup>121</sup>, and the photocatalytic performance of this nanocomposite was evaluated under sunlight exposure. (Fig.12). The experimental findings indicated that the  $\text{CuFe}_2\text{O}_4@\text{rGO}$  (10 wt.%) nanocomposite exhibited the highest photocatalytic efficiency in degrading tetracycline.

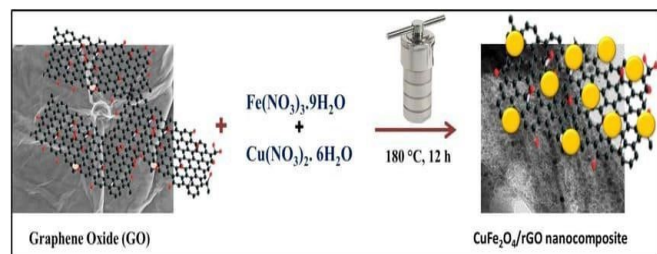


Fig.12 Schematic diagram showing the synthesis of  $\text{CuFe}_2\text{O}_4@\text{rGO}$  nanocatalyst. Reproduced from ref.121 with permission from John Wiley and Sons, copyright 2023

In 2016, Disi Qiao *et al.*<sup>122</sup> reported the photocatalytic degradation of Tetracycline using a  $\text{Fe}_3\text{O}_4@\text{GO}@\text{ZnO}$  magnetic nanocomposite, where graphene oxide served as the framework to enhance electron transfer, and ZnO functioned as an effective photocatalyst, achieving a 74% degradation of

tetracycline hydrochloride under visible light irradiation within 100min. The catalyst was found to be effective up to four cycles of use. A more efficient magnetic nanocomposite,  $\text{C}_3\text{N}_4@\text{MnO}_2@\text{GO}$ , synthesized by Chunyan Du *et al.*<sup>123</sup> in 2021, demonstrated an improved ability to photodegrade tetracycline hydrochloride under visible light, reaching a degradation rate of 91.4% in just 90 min.

As demonstrated by Shi *et al.*<sup>124</sup> the photo-Fenton degradation of tetracycline (TC) using a  $\text{CdS}@\text{reduced graphene (rGO)}@\text{ZnFe}_2\text{O}_4$  (ZFO) nanocomposite system under visible light exposure, a TC removal of 80% and 59.2% mineralization can be achieved.



[Type here]

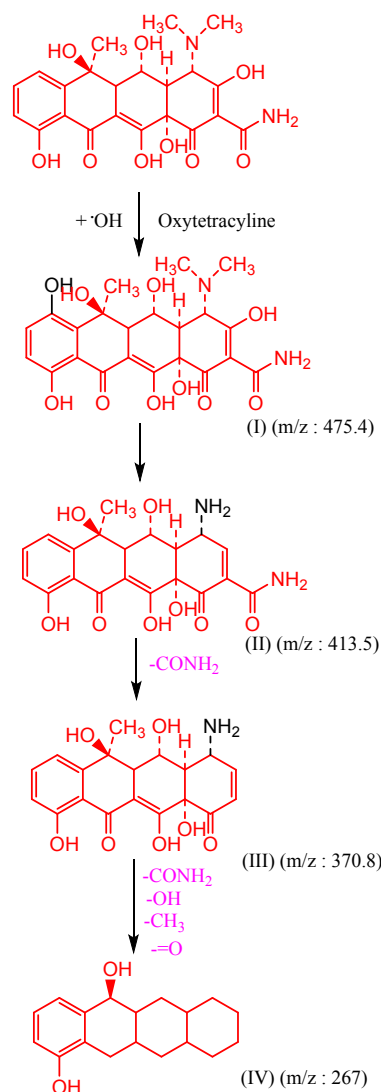


Fig.13 Diagrammatic representation of the proposed mechanism for the degradation of oxytetracycline under solar irradiation using  $\text{Co}_3\text{O}_4@\text{TiO}_2@\text{GO}$  photocatalyst.

The  $\text{Co}_3\text{O}_4@\text{TiO}_2$  graphene oxide nanocomposite synthesized by Jo *et al.*<sup>125</sup> through sol-gel and hydrothermal methods exhibited an excellent performance for the photocatalytic degradation of oxytetracycline under solar and visible light, achieving 91% efficiency in 90 min attributed to improved photoinduced charge separation and associated hydroxyl radical formation (Fig.13).

Recently, a novel photocatalyst composed of magnetic porous cobalt ferrite@rGO (CF@rGO) balls has been synthesized by Wang *et al.* using a modified microfluidic method (Fig.14). The resulting photocatalyst (CF@rGO) exhibited remarkable stability in cyclic experiments with great magnetic separability and has been effectively used for the photodegradation of oxytetracycline achieving the degradation efficiency of 84.7%<sup>126</sup>.

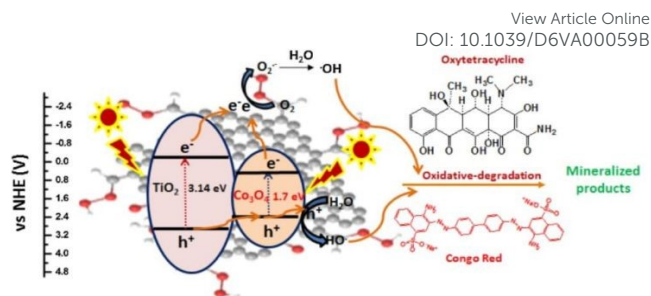


Fig.14 Schematic diagram of photocatalytic degradation of Oxytetracycline and Congo Red under solar irradiation. Reproduced from ref.126 with permission from Elsevier, copyright 2017

Numerous studies have shown that graphene oxide magnetite ( $\text{GO}@\text{Fe}_3\text{O}_4$ ) works as an effective photocatalyst for the degradation of ciprofloxacin in water using visible light, achieving efficiencies between 80-90% under optimal conditions of pH and  $\text{MO}@\text{GO}$  concentration<sup>127,128</sup>. The photocatalytic properties of this catalyst can be further improved by incorporating  $\text{TiO}_2$  nanoparticles, as illustrated in the research conducted by Uruş *et al.*<sup>129</sup>, where the  $\text{GO}@\text{Fe}_3\text{O}_4@\text{TiO}_2$  nanocomposite was synthesized using an in-

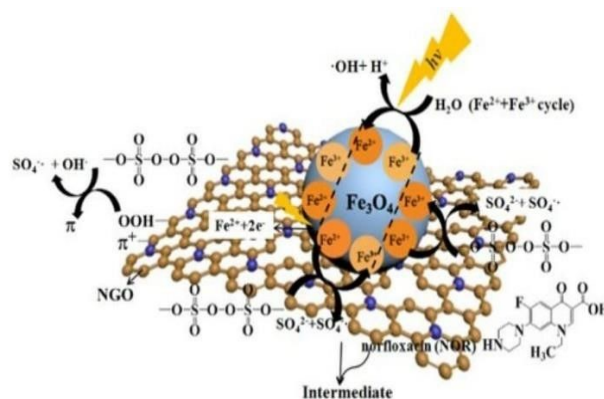


Fig. 15 Schematic representation of the photocatalytic degradation of norfloxacin using a nitrogen-doped reduced graphene oxide@ $\text{Fe}_3\text{O}_4$  nanocomposite. Reproduced from ref.131 with permission from Taylor & Francis, copyright 2020

situ method that successfully removed 91.5% of ciprofloxacin from water in 240 min.

A similar study conducted by Farhadian *et al.*<sup>130</sup> utilized a  $\text{TiO}_2@\text{Fe}_2\text{O}_3@\text{GO}$  nanocomposite for the degradation of metronidazole in aqueous conditions under UV light irradiation. Under optimal conditions of 10 mg/L metronidazole concentration, photocatalyst concentration of 1 g/L, irradiation of 120 min and a pH of 5 an efficiency of 97% is achieved. Focusing on the degradation of norfloxacin with activated peroxodisulfate (Fig.15). Wu *et al.*<sup>131</sup> investigated a UV-assisted



nitrogen-doped reduced grapheneoxide@Fe<sub>3</sub>O<sub>4</sub> composite created through a simple hydrothermal-co-precipitation method. At a pH of 3.0, 100% degradation of norfloxacin was achieved within 13 min.

Working on a similar line, Kakavandi *et al.*<sup>132</sup> developed a ternary nanocomposite by integrating TiO<sub>2</sub> nanoparticles with a magnetic core-shell structure onto rGO to form Fe<sub>3</sub>O<sub>4</sub>@SiO<sub>2</sub>@TiO<sub>2</sub>@rGO (FST@rGO). This photocatalyst was then used to degrade metronidazole (MNZ) antibiotic through the photocatalytic activation of peroxydisulphate (PDS) in a batch environment. The results showed the remarkable effectiveness of FST@rGO in the photodegradation of metronidazole across a wide range of pH. Under ideal conditions (pH: 7, PDS: 3nM and FST@rGO: 0.1g/L), over 94% of MNZ and 58% of total organic carbon was removed within 60 minutes of exposure to UV light (Fig.16).

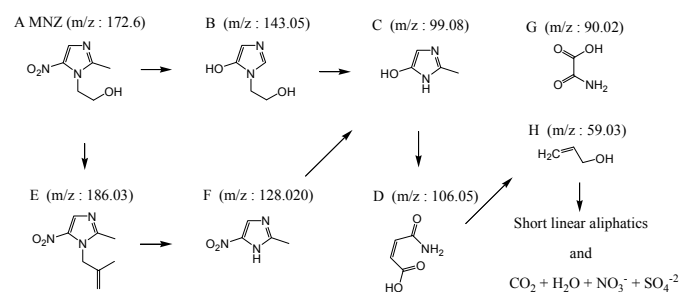


Fig.16 The proposed reaction mechanism for the degradation of metronidazole

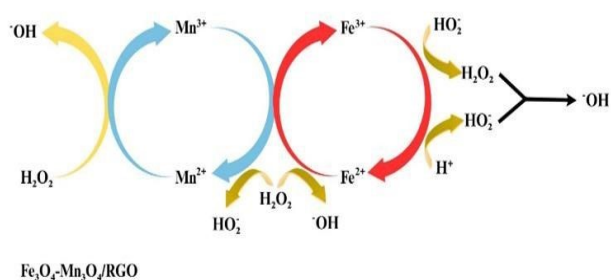


Fig.17 Diagrammatic representation of the ROS formed during the photocatalytic degradation of sulfamethazine using a Fe<sub>3</sub>O<sub>4</sub>@Mn<sub>3</sub>O<sub>4</sub>rGO nanocomposite

Wan *et al.*<sup>133</sup> showed that Fe<sub>3</sub>O<sub>4</sub>@Mn<sub>3</sub>O<sub>4</sub>-rGO NCs serves as an effective photocatalyst for the degradation of sulfamethazine in an aqueous solution (Fig.17). Under optimal conditions of 0.5

g<sup>L</sup>-<sup>1</sup> photocatalyst concentration, 0.07 mm L<sup>-1</sup> sulfamethazine at pH 3, a temperature of 35 °C, and 6 mmol L<sup>-1</sup> concentration of H<sub>2</sub>O<sub>2</sub> a photodegradation efficiency of 98% for sulfamethazine was observed. A novel photocatalyst, ZnO@Fe<sub>3</sub>O<sub>4</sub>-GO@ZIF, combining the features of magnetic graphene oxide and metal-organic frameworks synthesized by Chen *et al.*<sup>134</sup>, exhibited rapid degradation of three antibiotics—metronidazole, sulfamethazine, and norfloxacin—under simulated solar radiation for 1h (Fig.18,19). This resulting photocatalyst could be recycled at least ten times without significant deactivation.

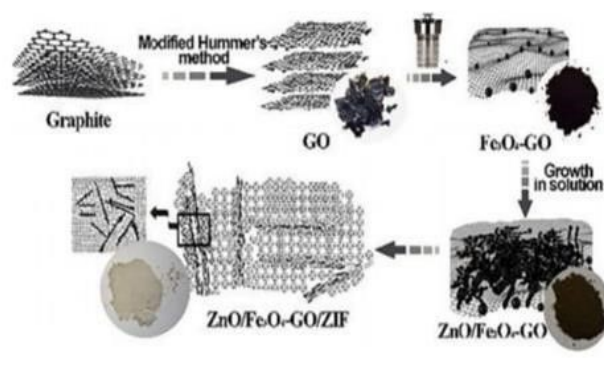


Fig.18 Synthesis of ZnO@Fe<sub>3</sub>O<sub>4</sub>-GO@ZIF nanocomposite. Reproduced from ref.134 with permission from Springer Nature, copyright 2021

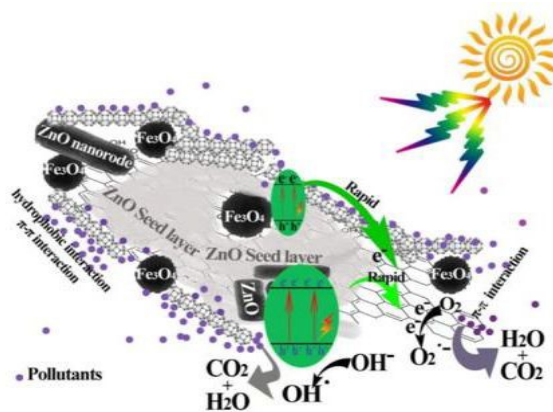


Fig. 19 Diagrammatic representation of the proposed mechanism for photocatalytic degradation of metronidazole, sulfamethazine and norfloxacin. Reproduced from ref.134 with permission from Springer Nature, copyright 2021

A slightly different approach was employed by Nimshi *et al.*<sup>135</sup> through a sonophotocatalytic degradation process. They synthesized CoFe<sub>2</sub>O<sub>4</sub>@TiO<sub>2</sub>@rGO (CoTG) ternary nanocomposite *via* cost effective and environment friendly green microwave and sol-gel methods. Pedalium murex plant's leaf extract served as the reducing and stabilizing agent during



[Type here]

the microwave synthesis. Its sonophotocatalytic degradation capabilities were examined against tetracycline and ciprofloxacin antibiotics in presence of ultrasonic irradiation and visible light. Impressive efficiencies of 92% and 84% for the degradation of Tetracycline (20 mg/L) and Ciprofloxacin (10 mg/L) in a short timeframe were demonstrated.

A magnetically separable core-shell heterostructured photocatalyst  $\text{Fe}_3\text{O}_4@\text{Bi}_2\text{O}_3@\text{RGO}$  was successfully synthesized for the first time through a self-assembly method by Zhu *et al.*<sup>136</sup>. In the degradation of quinolone antibiotics (QAs) under visible light irradiation, the synthesized  $\text{Fe}_3\text{O}_4@\text{Bi}_2\text{O}_3@\text{RGO}$  nanocomposites displayed an expanded range of visible light absorption, enhanced efficiency in charge separation, excellent photocatalytic performance and cyclic stability. The degradation rate of ciprofloxacin (CIP) using this photocatalyst reached an impressive 98.3% within 240 min, remaining above 80% even after ten photocatalytic reaction cycles.

Mehralipour *et al.*<sup>52</sup> synthesized an  $\text{rGO}@\text{Fe}^0@\text{Fe}_3\text{O}_4@\text{TiO}_2$  nanocomposite *via* Hummer's method and a straightforward sol-gel approach to study photocatalytic degradation of penicillin G in aqueous media (Fig.19). Using central composite design nanocomposite dosage (10–20 mg/L), pH (4–8), penicillin G concentration (50–100 mg/L and reaction time (30–60 min), were optimized and an efficacy of 96% was achieved at catalyst dose = 18.5 mg/L, pH=6.5, penicillin G concentration = 52 mg/L and reaction time = 59.1 min. Besides being magnetically retrievable the catalyst displayed high recyclability upto 5 cycles.

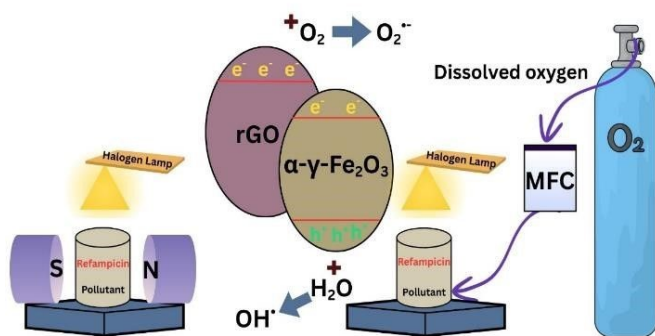


Fig.20 Schematic representation of the removal of rifampicin using  $\text{rGO}@\alpha\text{-}\gamma\text{-Fe}_2\text{O}_3$  assisted by an external magnetic field and dissolved oxygen

In a separate investigation, the engineered  $\text{Rgo}@\alpha\text{-}\gamma\text{-Fe}_2\text{O}_3$  exhibited remarkable photodegradation efficiency for the antibiotic rifampicin, achieving a degradation rate of 82.1% within 80 min of light exposure, utilizing 0.2 mg/ml of the  $\text{rGO}@\alpha\text{-}\gamma\text{-Fe}_2\text{O}_3$  based photocatalyst<sup>137</sup> (Fig.20).

#### 4.1.2 Antipyretics

Antipyretics are compounds which are used to alleviate fever<sup>139</sup>. They have become emerging environmental pollutants, largely due to their extensive use and subsequent discharge into wastewater. In particular, acetaminophen (paracetamol) poses a significant threat due to its widespread use and discharge into water bodies. It has been detected in wastewater, surface waters and in drinking water *via* oxidative conversion it is converted into N-acetyl-p-benzoquinone imine which results in toxicity. The stable chemical structure of acetaminophen is a major obstacle to its elimination through standard wastewater treatment techniques. The high solubility of antipyretics contributes to their widespread occurrence in wastewater treatment facilities, where they can endanger both the environment and public health.<sup>140-142</sup>. As a result, there is an increasing emphasis on eliminating them from water through photocatalysis.

Despite limited research on the degradation of antipyretic medications utilizing magnetic graphene oxide-based nanocomposites, the investigation conducted by Chen *et al.*<sup>134</sup>, highlighted the remarkable degradation of acetaminophen (paracetamol) using the  $\text{ZnO}@\text{Fe}_3\text{O}_4\text{-GO}@\text{IF}$  nanocomposite under solar irradiation for 1 h.

In a similar approach, Santosh Kumar *et al.*<sup>143</sup> using the chemical reflux method developed iron oxide nanorods uniformly coated on polypyrrole/reduced graphene oxide ( $\text{Fe}_3\text{O}_4@\text{PPy}@\text{rGO}$ ) nanohybrids. Photocatalytic studies under visible light indicated that the  $\text{Fe}_3\text{O}_4@\text{PPy}@\text{rGO}$  nanohybrids in the presence of persulfate achieved an 84% degradation of acetaminophen (ACP).

#### 4.1.3 Psychopharmaceuticals

Psychopharmaceuticals are drugs that exert therapeutic effects on the central nervous system influencing the pathological changes in experiences and behaviours associated with mental disorders. They include five basic categories: antipsychotics, antidepressants, stimulants, mood stabilizers, and anxiolytics<sup>144</sup>. Psychopharmaceuticals and related illicit substances designed to interact with the human nervous system may also have the potential to affect the nervous systems of non-target organisms, potentially leading to adverse ecological consequences that alter their physiology and behaviour. Therefore, their removal from aquatic environments is crucial<sup>145,146</sup>. The photocatalytic degradation of these substances using magnetic graphene oxide-based nanocomposites is illustrated in this section.

A magnetically recyclable  $\text{GO-TiO}_2$  composite, as reported by Linley *et al.* in 2014<sup>147</sup> within 60 min under UV irradiation achieved up to 99% removal of carbamazepine and caffeine

from aqueous solutions. This composite demonstrated superior photocatalytic activity compared to commercial P25, while also offering the benefits of high recoverability and reusability.



The graphene oxide-based magnetic photocatalyst  $\text{Fe}_3\text{O}_4@\text{GO}$ , as proposed by da Silva *et al.*<sup>148</sup>, exhibited exceptional efficiency in treating water contaminated with clonazepam through photo-Fenton degradation (Fig.21,22).

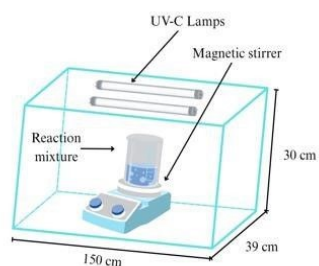


Fig. 21 Diagrammatic representation of the photoreactor used in the study by Da Silva *et al.*<sup>121</sup>

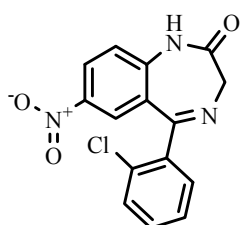


Fig.22 Molecular structure of clonazepam

The rGO-loaded-magnetite composites synthesized by Moztahida *et al.*<sup>149</sup> using a cost-effective co-precipitation method demonstrated remarkable efficiency in the photodegradation of carbamazepine. The hybrid composite highlighted a high photodegradation ability of 98.7% within 3 h at a pH of 6.5 (Fig.23,24,25).

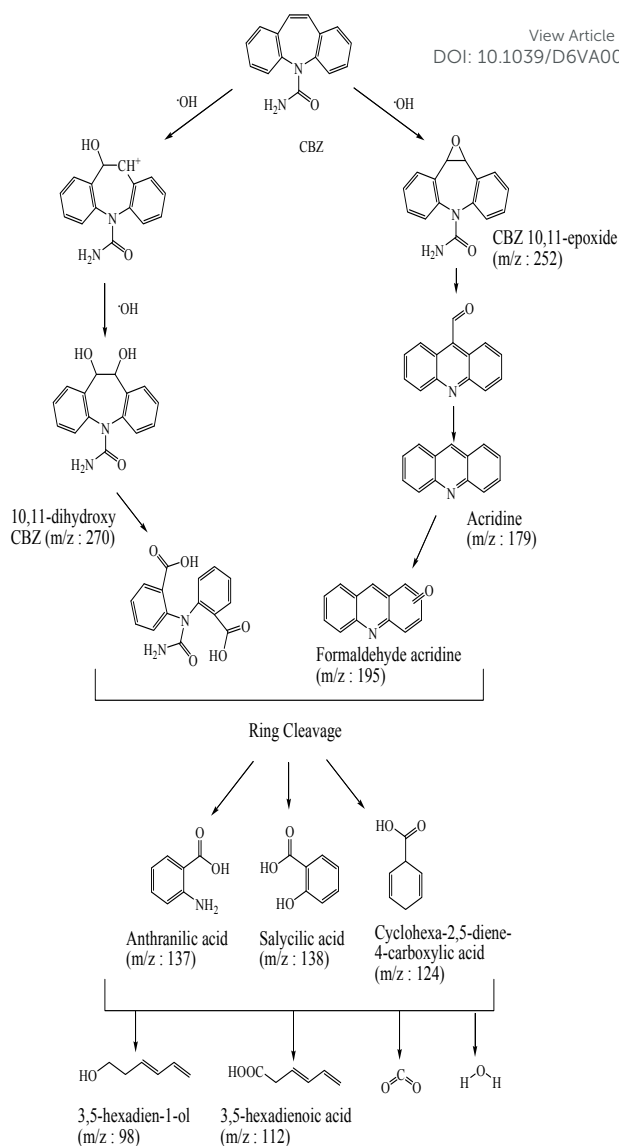


Fig.23 Pathway of carbamazepine degradation and the intermediates formed.



[Type here]

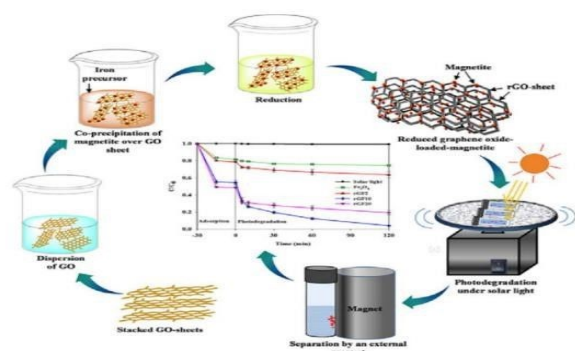


Fig.24 Schematic representation of the process of synthesis of rGO loaded-magnetite, its role as photocatalyst in the degradation of carbamazepine and its separation using an external magnet. Reproduced from ref.149 with permission from Elsevier, copyright 2019

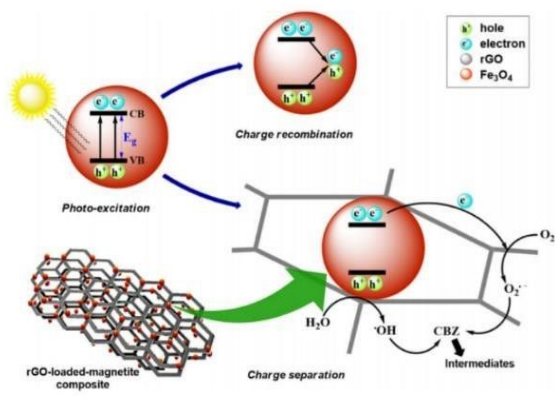


Fig. 25 Proposed mechanism for the production of ROS during the photocatalytic degradation of carbamazepine. Reproduced from ref.149 with permission from Elsevier, copyright 2019

#### 4.1.4 Estrogens

Estrogens are the primary female sex hormones, responsible for regulating the development of secondary sexual characteristics and the female reproductive system. They can be used therapeutically for treating different endocrine related disorders. However, their inappropriate use and release into the environment can lead to pollution. Estrone (E1), 17 $\beta$ -estradiol (E2), estriol (E3), and 17- $\alpha$  ethynyl estradiol (EE2) are some of the examples of estrogens that carry substantial environmental hazards<sup>150</sup>. These estrogens are found in trace amounts in the environment, such as in soil, surface water, or seawater, and have been associated with breast cancer, ovarian cancer, fish feminization, low sperm count in adult males, endometriosis, obesity, cardiovascular endocrinology, and fibroids<sup>151,152</sup>. This highlights the importance of successfully removing them from the environment.

According to a research by Ajibola A. Bayode *et al.*<sup>153</sup> the steroid hormones estrone, 17 $\beta$ -estradiol, estriol, and ethinyl estradiol were successfully oxidized and mineralized using a photocatalytic nanocomposite composed of kaolinite, pulverized carica papaya seeds, 3-aminopropyltriethoxysilane (APTES), hematite (Fe<sub>2</sub>O<sub>3</sub>), and graphene oxide (GO). Even when all estrogens were present in the same water sample, the use of this photocatalytic nanocomposite still resulted in more than 80% steroid estrogen oxidation (Fig.26).

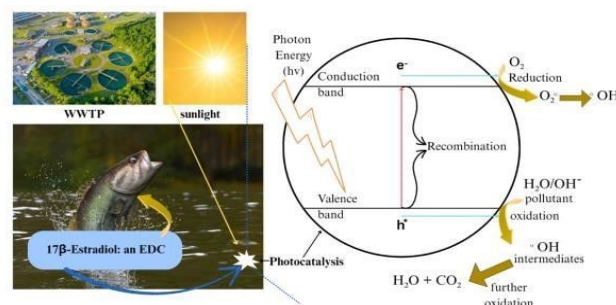


Fig.26 Schematic illustration depicting the photodegradation of harmful estrogen present in aqueous media

Reusable, magnetically separable ZnFe<sub>2</sub>O<sub>4</sub>-Ag/rGO nanocomposite (NC) were synthesized by Khadgi *et al.*<sup>154</sup> by co-modifying ZnFe<sub>2</sub>O<sub>4</sub> with GO and Ag nanoparticles (NPs) through a simple one-pot hydrothermal method. Under visible light the photocatalytic performance of the catalyst was evaluated for successful degradation of 17 $\alpha$ -ethynylestradiol (EE2). Under visible light irradiation 80% degradation of 17 $\alpha$ -ethynylestradiol was achieved. Reusability upto 5 cycles showed a decline in photocatalytic activity from 100 to 70%.

#### 4.1.5 Antidiabetic drugs

Antidiabetic drugs are the those which are used in the management of diabetes or high blood glucose levels in the body. With the increase in the prevalence of diabetes in the past few decades the demand for these drugs has increased dramatically. For diabetes mellitus type II, metformin (Met) has proven to be a convenient and effective pharmaceutical treatment. Unlike plenty of other pharmaceutical drugs, it is not metabolised by humans rather it passes through the body unaltered and enters aquatic compartments such as in sewage<sup>155</sup>. But by conventional wastewater treatment, these drugs are not effectively removed and end up in surface, ground and even drinking water. This poses potential risks to aquatic ecosystems and potentially to human health<sup>156,157</sup>. The degradation of metformin *via* magnetic metal oxide / graphene oxide-based nanocomposites holds good promise in their removal from the environment.

Khavar *et al.*<sup>158</sup> synthesized a novel hybrid nanostructured spherical catalyst, Fe<sub>3</sub>O<sub>4</sub>@rGO@ZnO/Ag-NPs (FGZAg), which under both ultraviolet and visible light irradiation effectively degraded metformin (MTF)(Fig.27). The fabrication of the



catalyst employed  $\text{Fe}_3\text{O}_4$  microspheres as templates, which were coated with GO and ZnO shells, followed by decoration with Ag nanoparticles (NPs), and finally annealed in a nitrogen atmosphere. The FGZA achieved 60% mineralization and complete degradation of  $20 \text{ mg L}^{-1}$  MTF within 60 minutes in the visible-light photocatalytic process.

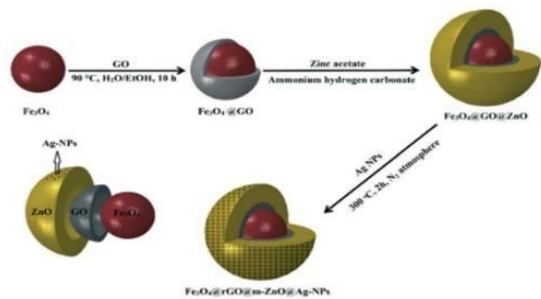


Fig.27 Schematic representation of the synthesis of onion-like  $\text{Fe}_3\text{O}_4@\text{rGO}@\text{ZnO}@\text{Ag}$  nanoparticles. Reproduced from ref.158 with permission from Royal Society of Chemistry, copyright 2019

## 4.2 Microplastics

Microplastics are defined as any particles made of plastic with a size smaller than  $5 \text{ mm}^{159}$ . They can be broadly divided into two categories based on their origin: primary and secondary microplastics. Primary microplastics are those that are manufactured and intentionally added to consumer and commercial products such as cosmetics, personal care items, pharmaceuticals, detergents, and insecticides. In contrast, secondary microplastics are the ones that arise unintentionally from the degradation of larger plastic materials through various physical, chemical, or biological processes, including items like plastic bottles, plastic bags, and food containers, fishing gear made from plastic<sup>160, 161</sup>. It is estimated that about 10 million tons of plastic waste enter the ocean annually ( UNESCO ) from various sources, with wastewater treatment plants (WWTPs), surface runoff from contaminated areas or disposal sites, and littering on beaches as the primary contributors<sup>162</sup>. The most widely used plastics globally include polyethylene (PE), low-density polyethylene (LDPE), high-density polyethylene (HDPE), polypropylene (PP), polystyrene (PS), and polyvinyl chloride (PVC), polyurethane, with many of these polymeric materials are difficult to recycle<sup>163</sup>.

The presence of microplastics in the environment poses a considerable threat to various living organisms, including microorganisms, humans, animals, and plants. Within the environment, microplastics disrupt both terrestrial and aquatic ecosystems<sup>164-169</sup>. In marine settings, they are consumed by a large number of diverse species. Microplastics can block the digestive tract, diminish food intake, harm the intestines, and

trigger oxidative stress, resulting in internal injuries, decreased nutrient absorption, and potentially death. Additionally, microplastics can inhibit plant and algae growth, photosynthesis, gene expression<sup>164-166</sup>. In soil, microplastics can modify water retention, alter soil structure, and negatively impact beneficial microorganisms, thereby reducing agricultural productivity and food security<sup>166</sup>.

Microplastics have also been detected in various tissues of both animals and humans, including blood, brain, placenta, and reproductive organs<sup>167, 168</sup>. They have even been identified in breast milk. In humans and animals, microplastics can lead to inflammation, oxidative stress, and disruption of the gut microbiome, which may result in gastrointestinal problems, liver damage, and potential endocrine and reproductive disorders<sup>167-169</sup>. Moreover, they can transport persistent toxic substances such as phthalates and bisphenol A, which may lead to further complications<sup>167-170</sup>. Thus, there is an urgent need to remove these contemporary pollutants from the environment. The removal of microplastics from water or wastewater involves challenges due to their inherent physical and chemical properties<sup>171</sup>. Microplastics can be degraded using several techniques, including biodegradation, chemical processes, and thermal treatment. While these methods may be effective for removing microplastics from water, they often require considerable time, financial investment and involve high energy demands<sup>172-174</sup>. Recently, the mineralization of microplastics through photodegradation has attracted significant attention among the scientific community, as it converts contaminants into non-hazardous compounds in a quick, effective, and cost-efficient manner.

Researchers have utilized  $\text{TiO}_2$ -based nanomaterials;  $\text{TiO}_2$ -rGO and titanium dioxide ( $\text{TiO}_2$ )/gold nanorods ( $\text{AuNRs}$ )@rGO for the efficient degradation of polypropylene and polystyrene through photocatalysis for environmental pollution mitigation<sup>175, 176</sup>.

In another study, the  $\text{In}_2\text{O}_3$ -rGO nanocomposite-based metal oxide exhibited efficient photocatalytic degradation of polyethylene films when exposed to visible light for varying durations of 0, 10, 20, 30, 40, and 50 h. A degradation efficiency of 99.47% was achieved in 50 h, as confirmed by thermogravimetric analysis<sup>177</sup>.



[Type here]

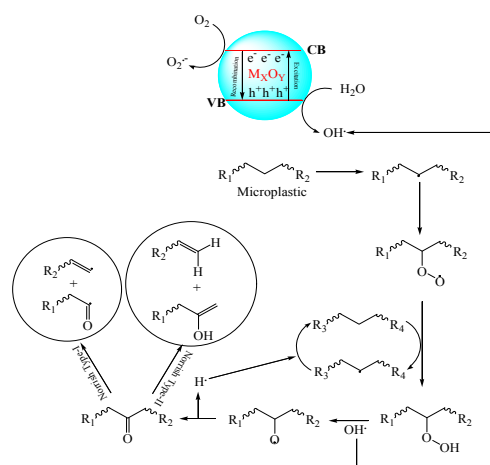


Fig.28 Photocatalytic mechanism for microplastic degradation under light irradiation using metal oxide semiconductors

A recent study by Uogintè *et al.* highlights the application of graphene oxide-based metal oxide nanomaterials for the effective removal of polyethylene microplastic particles through photocatalytic degradation<sup>178</sup>

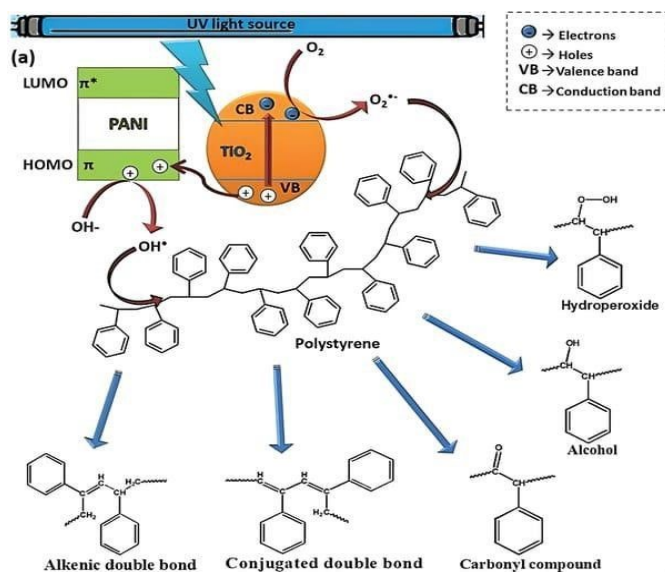


Fig.29 Schematic diagram of the proposed mechanism for polystyrene photodegradation using TiO<sub>2</sub>-PANI nanocomposites as catalyst. Reproduced from ref.179 with permission from John Wiley and Sons, copyright 2023

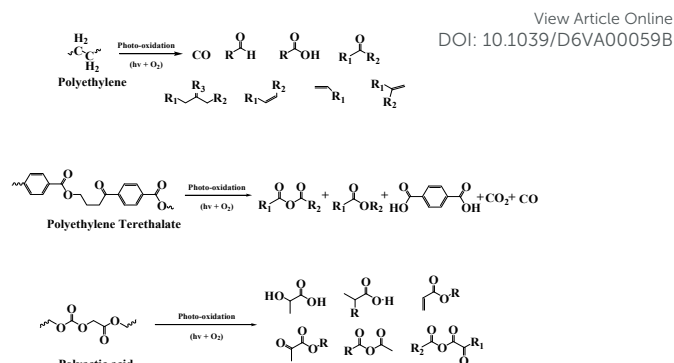


Fig.30 Photocatalytic degradation mechanisms of polyethylene, polyethylene terephthalate and poly(lactic acid).

The use of magnetic metal oxide@graphene oxide in photocatalytic degradation of microplastic has been introduced quite recently which requires further investigation for its practical implementation. Nevertheless, there are numerous studies reported in literature that show great potential for its application. For instance, TiO<sub>2</sub> and ZnO nanoparticles, along with their nanocomposites comprising pure metals, metal sulfides, C and N dopants, heterojunctions, and organic frameworks, have been demonstrated to exhibit remarkable efficiency under optimal conditions of irradiation, pH, and concentration in degrading polythene (PE), polypropylene (PP), polystyrene (PS), polyethylene terephthalate (PET), and polyvinyl chloride (PVC) (Fig. 28,29,30). In addition to TiO<sub>2</sub> and ZnO, other photocatalysts like CeO<sub>2</sub>, Fe<sub>2</sub>O<sub>3</sub>, and CuO@BiVO<sub>4</sub> have also been found effective for degrading microplastics from water samples<sup>175,179-180</sup>.

Therefore, the findings reported in the existing literature support the concept of utilizing magnetic metal oxide@graphene oxide-based nanocomposites for the elimination of microplastics from water, with the added benefits of easier recovery, enhanced efficiency and reusability, thus making this a promising area of research.

### 4.3 Pesticides

In recent decades, the use of pesticides in agriculture has significantly increased due to the need to ensure higher crop yields and protect plants from pests, diseases, and weeds. While pesticides have contributed to food security, their excessive and indiscriminate application has led to serious environmental and health concerns. Many pesticides are persistent organic pollutants (POPs) that accumulate in soil, water bodies, and the food chain, resulting in toxicity to non-target organisms, including beneficial insects, birds, aquatic life, and even humans. Exposure to these chemicals has been linked to neurological disorders, endocrine disruption, and carcinogenic



effects<sup>181, 182</sup>. In response to these challenges, researchers have turned to nanotechnology-based solutions, particularly graphene oxide (GO)-based nanocomposites, for the remediation of pesticide-contaminated environments. Graphene oxide possesses a high surface area, excellent adsorptive capacity, and functional groups that can facilitate catalytic degradation reactions. When incorporated with metal or metal oxide nanoparticles, GO-based nanocomposites act as highly efficient photocatalysts under visible light, breaking down complex pesticide molecules into less harmful or inert compounds. This approach offers a promising, sustainable strategy for mitigating the environmental impact of pesticides while ensuring agricultural productivity<sup>183,184</sup>.

Dehghan *et al.*<sup>185</sup> synthesized an rGO@Fe<sub>3</sub>O<sub>4</sub>@ZnO nanocatalyst *via* the thermal co-precipitation method and further used to study the oxidative degradation of the pesticide. Metalaxyl in aqueous solution under vis-light irradiation. It was found that under optimized conditions, a degradation of 92.11% was obtained in 120 min., along with good reusability and reduced toxicity of Metalaxyl.

For the degradation of chlorpyrifos, an organophosphate pesticide, under visible light Zangiabadi and co-workers<sup>186</sup> synthesized GO@Fe<sub>3</sub>O<sub>4</sub>@TiO<sub>2</sub> mesoporous nanocomposites as nanocatalysts. The nanocomposite showed great promise, achieving 97% degradation of the pesticide under investigation in 60 min. It also showed good catalytic activity after repeated runs. As it shows the possible degradation mechanism.

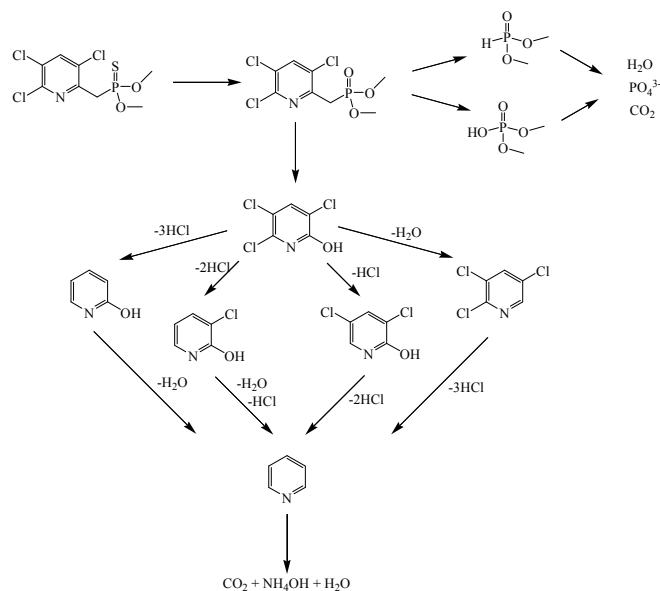


Fig. 31 A possible mechanism for the degradation of chlorpyrifos<sup>View Article Online DOI: 10.1039/D6VA00059B</sup>. The degradation of chlorpyrifos under UV light was studied by Gupta *et al.*<sup>106</sup> who synthesized an rGO@CoFe<sub>2</sub>O<sub>4</sub>@TiO<sub>2</sub> photocatalyst using co-precipitation and modified Hummer's method (Fig.31,32,33). The nanocomposite showed good catalytic activity for the degradation of the given organophosphate pesticide along with good reusability.

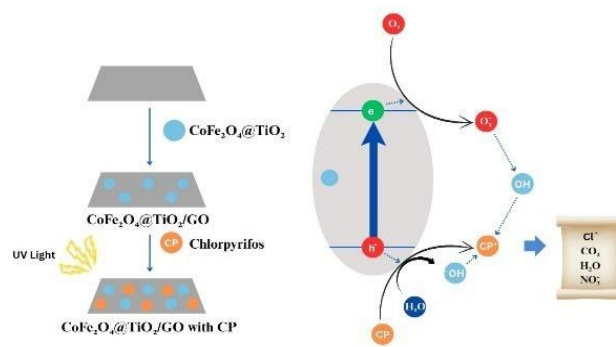


Fig.32 Photocatalytic degradation mechanism of chlorpyrifos using rGO@TiO<sub>2</sub>@CoFe<sub>2</sub>O<sub>4</sub> nanocomposite.

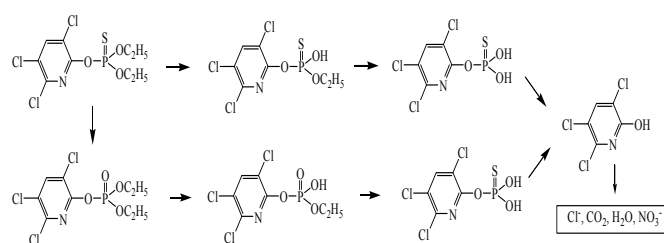


Fig. 33 Degradation pathways of chlorpyrifos using rGO@TiO<sub>2</sub>@CoFe<sub>2</sub>O<sub>4</sub> nanocomposite.

The degradation of another pesticide, diazinon, was evaluated in a study by Naynava *et al.*<sup>187</sup> using a GO@Fe<sub>3</sub>O<sub>4</sub>@CeO<sub>2</sub> hetero junction based photocatalyst under visible light irradiation. The use of the nanocomposite showed great promise, degrading 97.9% of the organophosphate pesticide in 60 min (Fig.34).



[Type here]

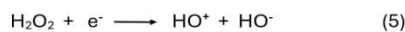
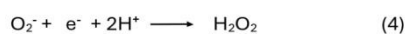
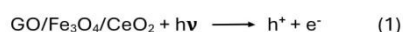


Fig.34 Reactions showing the degradation pathway of diazinon

The excessive use of herbicides in agriculture has been a growing problem due to the difficulties in removing them from the environment. Boruah and Das<sup>188</sup> studied the photometric detection and degradation of atrazine, a chlorinated herbicide belonging to the class of triazines, using an rGO@Fe<sub>3</sub>O<sub>4</sub>@TiO<sub>2</sub> nanocomposite prepared using the one-step hydrothermal method. The results indicated that the nanocomposite showed

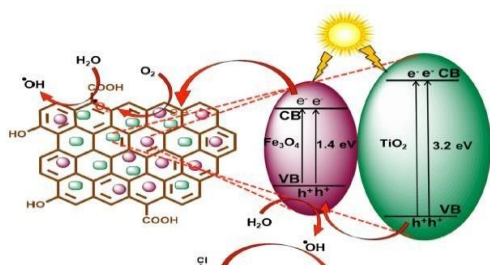


Fig.35 Photocatalytic degradation of atrazine represented schematically. Reproduced from ref.188 with permission from Elsevier, copyright 2020

impressive capability to photocatalytically degrade the atrazine molecule, degrading 100% of the herbicide under natural sunlight irradiation (Fig.35). The removal of the organochlorine insecticides aldrin and dieldrin from surface water using magnetically retrievable nanocomposites was investigated by Akçağlar<sup>189</sup>, who synthesized a GO@CuFe<sub>2</sub>O<sub>4</sub>@TiO<sub>2</sub> photocatalyst using hydrothermal and Hummer's method (Fig.36). It was found that under optimal conditions, photodegradation efficiencies of 100% and 99% were achieved for aldrin and dieldrin respectively, along with impressive reusability.

Nasiripur *et al.*<sup>190</sup> studied the photocatalytic degradation of the organophosphate insecticide parathion methyl using a GO@Fe<sub>3</sub>O<sub>4</sub>@Bi<sub>2</sub>MoO<sub>6</sub> nanocomposite (Fig.37,38).

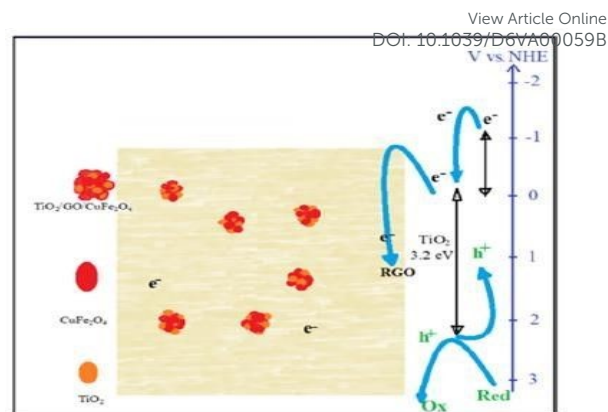
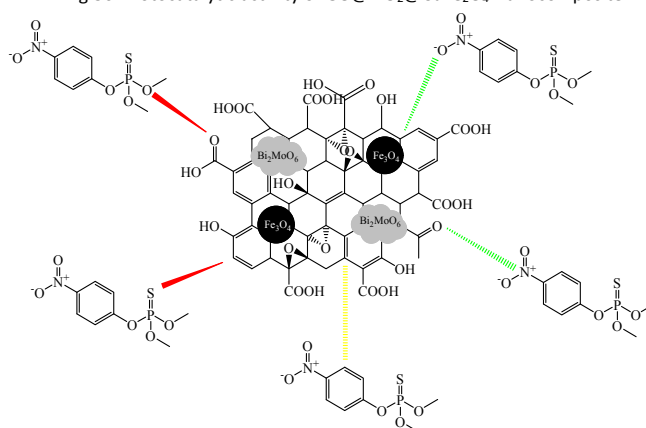
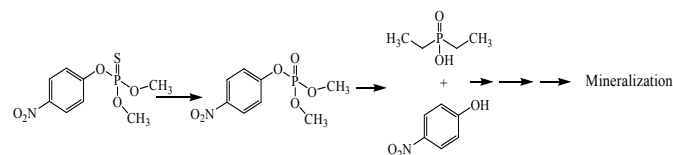
Fig.36 Photocatalytic activity of GO@TiO<sub>2</sub>@CuFe<sub>2</sub>O<sub>4</sub> NanocompositeFig. 37 Possible interaction between methyl parathion and GO@Fe<sub>3</sub>O<sub>4</sub>@Bi<sub>2</sub>MoO<sub>6</sub> nanocomposite

Fig.38 Products obtained from photocatalytic degradation of methyl parathion.

Under suitable conditions, 95% of parathion methyl was degraded under visible light irradiation in 120 min. Binary nanocomposites containing magnetic oxides and ferrites in conjunction with GO have also been studied for the degradation of pesticides in aqueous media.

Tabasum and co-workers<sup>191</sup> designed GO@MnFe<sub>2</sub>O<sub>4</sub> and GO@NiFe<sub>2</sub>O<sub>4</sub> binary photocatalysts for the study of acetamidrid, an odourless neonicotinoid pesticide, under UV methylene blue (MB) in waste water using a GO@MgFe<sub>2</sub>O<sub>4</sub>@CuO nanocomposite through microwave-ultrasonic procedure. The synthesised photocatalysts showed excellent degradation capacity, degrading >90% of the pesticide in 27 min.

In similar research, Tabasum *et al.*<sup>192</sup> synthesized GO@Fe<sub>3</sub>O<sub>4</sub> and GO@CoFe<sub>2</sub>O<sub>4</sub> nanocomposites to study the degradation of



the same pesticide. It was found that the ferrite and magnetite photocatalysts degraded approximately 97% and 90% of acetamidrid pesticide respectively, in 60 min of UV light irradiation.

Khoj *et al.*<sup>193</sup> synthesized a GO@Fe<sub>3</sub>O<sub>4</sub> binary nanocomposite and utilised it to investigate the degradation of the organophosphate pesticide diazinon. 99% of diazinon degradation was observed under 50 min. of UV-light irradiation. Persulphate-activated GO@Fe<sub>3</sub>O<sub>4</sub> nanocomposites were prepared by Dolatabadi *et al.*<sup>194</sup> for the study of the degradation of the organophosphate insecticide malathion in groundwater samples. The photocatalyst showed excellent capacity as a degrading agent, showing a degradation efficiency of 96.5% in 30 min. of reaction.

Deviating slightly from standard research, Soltani-nezhad and coworkers<sup>195</sup> synthesized a quaternary nanocomposite GO@Fe<sub>3</sub>O<sub>4</sub>@TiO<sub>2</sub>-NiO and studied the photocatalytic degradation of the pesticide imidacloprid under varying conditions of pH and nanocatalyst and pesticide concentration. The results showed that under optimal conditions (pH: 9, 0.1 g nanocatalyst, and 25 ppm pesticide), 94.61% degradation was observed under visible light irradiation.

#### 4.4 Dyes

The widespread rise in the use of artificial dyes, particularly in the textile, leather, paper, and cosmetic industries, has been driven by their bright colours, stability, and cost-effectiveness. However, this increased usage has led to significant environmental challenges. Many synthetic dyes are non-biodegradable and persist in the environment, especially in water bodies, where they reduce light penetration, hinder photosynthesis, and disrupt aquatic ecosystems. Additionally, several dyes and their degradation products are toxic, mutagenic, or even carcinogenic, posing serious health risks to humans and animals. Conventional methods for dye removal, such as coagulation, flocculation, or adsorption using activated carbon, often have limitations in efficiency and cost<sup>196,197</sup>. In recent years, graphene oxide (GO)-based nanocomposites have emerged as promising materials for the degradation of artificial dyes. Due to GO's high surface area, abundant functional groups, and excellent dispersibility in aqueous media, it serves as an effective support for metal and metal oxide nanoparticles. These nanocomposites can act as powerful photocatalysts under sunlight or visible light, accelerating the breakdown of complex dye molecules into less harmful compounds. This green and efficient approach offers a sustainable solution to mitigate the environmental impact of artificial dye pollution<sup>198,199</sup>.

Waheed *et al.*<sup>200</sup> studied the photocatalytic degradation of methylene blue (MB) in wastewater using a GO@MgFe<sub>2</sub>O<sub>4</sub>@CuO nanocomposite synthesized through a microwave-ultrasonic procedure. The synthesized nanocatalyst, under optimal conditions, showed a degradation efficiency of 98.8% in 27 min., and also showed good reusability upto four cycles of the photocatalytic degradation process.

Benjwal *et al.*<sup>201</sup> investigated the photocatalytic degradation of MB using binary rGO@TiO<sub>2</sub> and rGO@Fe<sub>3</sub>O<sub>4</sub> as well as tertiary rGO@Fe<sub>3</sub>O<sub>4</sub>@TiO<sub>2</sub> nanocomposites synthesized from a one-step solvothermal process, and the catalytic activity of each nanocomposite was compared. Under visible and UV light

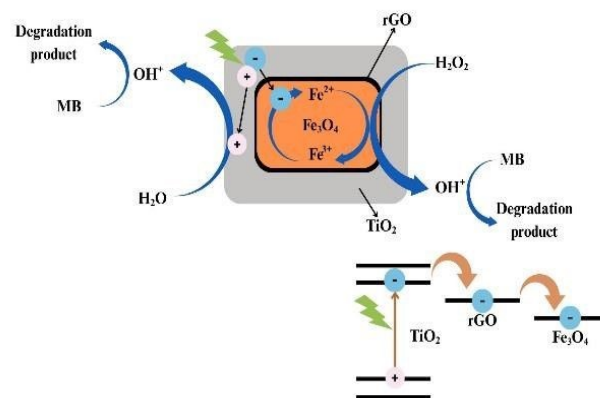


Fig.39 Suggested mechanism for methylene blue degradation by rGO@Fe<sub>3</sub>O<sub>4</sub>@TiO<sub>2</sub> nanocomposite

irradiation, 100% and 91% of MB degradation were observed respectively, within 5 min. for the ternary nanocomposite, showcasing its superior capability as a photocatalyst in comparison to binary nanocomposites.

Banerjee and co-workers<sup>202</sup> also conducted the experiment using the same dye and ternary nanocomposite. Different component ratios of the rGO@Fe<sub>3</sub>O<sub>4</sub>@TiO<sub>2</sub> photocatalyst were synthesized using sol-gel and wet assembly methods. It was found that the composite possessing the ratio 1:1:2 of rGO, Fe<sub>3</sub>O<sub>4</sub> and TiO<sub>2</sub> showed the highest degradation of MB, degrading 99% and 94% of the sample under UV and visible light irradiation respectively (Table 2, Fig.39).

Table 2: Photocatalytic degradation efficiencies of different rGO@Fe<sub>3</sub>O<sub>4</sub>@TiO<sub>2</sub> nanocomposites.



[Type here]

Nanocomposites	Photocatalytic degradation of MB in UV/ Visible	
	C/C <sub>0</sub> (%) (in 9 min.)	C/C <sub>0</sub> (%) (in 6 min.)
GFT1	87	90
GFT2	93	95
GFT3	90	88
GFT4	90	97
GFT5	88	92
GFT6	94	99
GFT7	93	97

In similar research, Nadimi *et al.*<sup>203</sup> independently conducted the same experiment, replacing rGO with GO. The nanocomposites were synthesized using modified Hummer's and ultrasonication methods while varying the amount of GO. It was found that the nanocomposite with the highest amount of

GO showed the greatest degradation of MB, with reported degradation percentages of 82% and 76% in 90 min of irradiation with UV and visible light respectively.

Bibi *et al.*<sup>204</sup> used the same rGO@Fe<sub>3</sub>O<sub>4</sub>@TiO<sub>2</sub> nanocomposite to study the photocatalytic degradation of the triarylmethane dye malachite green (MG) under UV-visible light. The conventional hydrothermal method was used to synthesize the photocatalyst. The results showed that, in comparison to pure TiO<sub>2</sub>, the nanocomposite showed much greater promise as a photocatalyst, degrading 99% of MG in 55 min. under visible light irradiation.

FFIGOjha and co-workers<sup>205</sup> investigated the photocatalytic degradation of azo-dye from aqueous medium under ambient conditions utilizing an rGO@Fe<sub>3</sub>O<sub>4</sub>@ZnO nanocomposite synthesized using hydrothermal method. The catalytic activity of the tertiary nanocomposites were compared to those of pure ZnO, pure Fe<sub>3</sub>O<sub>4</sub>, ZnO@Fe<sub>3</sub>O<sub>4</sub> and Fe<sub>3</sub>O<sub>4</sub>@GO systems. It was found that the nanocomposites showed superior degradation capability, attributed to the synergistic effect of the components of the nanoparticles, degrading approximately 97% of the azo-dye within 150 min on visible light irradiation.

Kumar *et al.*<sup>206</sup> synthesized GO@CuFe<sub>2</sub>O<sub>4</sub>@ZnO nanocomposites using a one-step combustion process (Fig.40) for the study of photocatalytic degradation of MB, the azo-dye methyl orange (MO) and the xanthene dye rhodamine-B (RhB). The separation ratio of the photogenerated electron-hole pairs was enhanced due to the generation of p-n junction between CuFe<sub>2</sub>O<sub>4</sub> and ZnO. The ternary nanocomposite showed great promise, degrading 99% of RhB in 50 min., 100% of MB in 40 min. and >90% of MO in 200 min.

The photocatalytic degradation of Bismarck Brown (BB) and Acid Orange 7 (AO) was studied by Boruah *et al.*<sup>85</sup> using an rGO@Fe<sub>3</sub>O<sub>4</sub>@V<sub>2</sub>O<sub>5</sub> nanocomposite synthesized through co-precipitation method. It was found that 94.5% of BB and 93.3%

of AO were degraded using the photocatalyst in 70 and 80 min. respectively.

Similar to the work on pesticides, binary nanocomposites composed of magnetic oxides or ferrites embedded in graphene oxide have also been studied for their role in the photocatalytic degradation of dyes in aqueous media. Baptistella *et al.*<sup>207</sup> studied the degradation of various dyes such as MB, Reactive Black 5 (RB) and Acid Blue 80 (AB) using a GO@Fe<sub>3</sub>O<sub>4</sub> binary nanocomposite. Degradation rates of 70%, 54% and 48% were obtained for MB, RB, and AB respectively.

GO-supported ferrites of Fe,Co and Ni (GO@FeFe<sub>2</sub>O<sub>4</sub>, GO@CoFe<sub>2</sub>O<sub>4</sub>, and GO@NiFe<sub>2</sub>O<sub>4</sub>) were synthesized by Sheshmani *et al.*<sup>208</sup> for the photocatalytic degradation of Remazol Black B (RBB). All three nanocomposites showed great promise as a photocatalysis for the decomposition of the dye under study. (Fig.41)

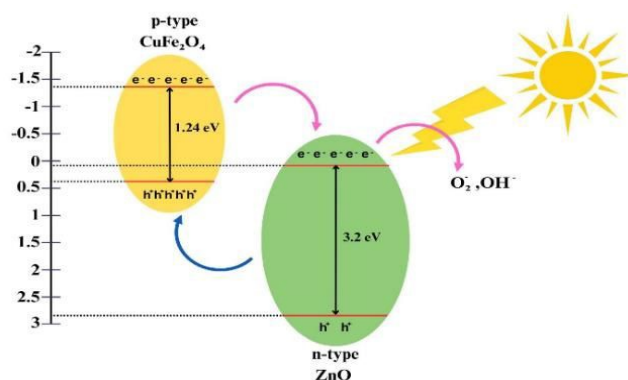


Fig.40 Diagrammatic representation of photocatalytic degradation of GO@ZnO@CuFe<sub>2</sub>O<sub>4</sub> nanocomposite

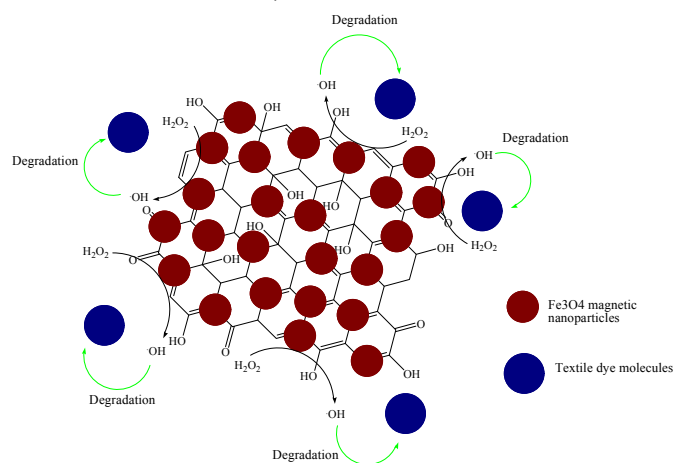


Fig. 41 Schematic representation for the possible photocatalytic degradation mechanism of dyes

## 5. Mechanism of Photocatalytic degradation

A detailed analysis of the mechanism involved in the photocatalytic degradation of various organic pollutants reveals/indicates that upon



light irradiation, the metal oxide semi-conductor component of the photocatalyst generates  $e^-/h^+$  pairs. These photo-generated electrons in the conduction band reduce oxygen to superoxide radicals ( $\bullet O_2^-$ ), and water to hydroxyl radicals ( $\bullet OH$ )<sup>209</sup>. Though the efficiency is reduced due to rapid recombination of these  $e^-/h^+$  pairs, to mitigate this challenge, graphene oxide or reduced graphene oxide (GO or rGO) plays a pivotal role. The incorporation of graphene oxide or reduced graphene oxide (GO or rGO) introduces an interfacial electron transfer pathway to facilitate the migration of photo-generated electrons from the metal oxides conduction band to GO. This electron trapping suppresses charge recombination leading to enhanced radical formation and consequently improved degradation efficiency<sup>210,211</sup>.

To understand the mechanism of action of these radical intermediates, many chemical species able to interact with them have been applied to various oxidative processes. Such substances are termed as "radical scavengers", capable of reacting quickly and specifically with a radical to form a stable species which does not interfere in the reaction. Various molecules have been studied for the radical scavenging of different intermediates: for example, holes in the valence band are scavenged using electron donating species such as ethylene glycol<sup>212</sup>, hydroxyl radicals ( $\bullet OH$ ) can be scavenged by flavonoids<sup>213</sup>, and superoxide ion radicals ( $\bullet O_2^-$ ) by ascorbic acid<sup>214</sup>. Scavengers would be useful in identifying the dominant active species responsible for the degradation of the pollutants and hence help in understanding the mechanistic pathway for the degradation.

Disi Qiao *et al.*<sup>122</sup> did mechanistic studies for photocatalytic degradation of Tetracycline using a  $Fe_3O_4@GO@ZnO$  nanocomposite using (5,5-Dimethyl-1-pyrroline-N-oxide) DMPO as a scavenger. They reported the presence of DMPO- $\bullet OH$  and DMPO- $\bullet O_2^-$  in the Electron Spin Resonance (ESR) spectra indicating the dual effects of  $\bullet OH$  radicals and  $\bullet O_2^-$  radicals during the photocatalytic degradation. Similar studies employing DMPA and TEMPO as scavengers were done on a  $C_3N_4@MnO_2@GO$  nanocomposite by Chunyan Du *et al.*<sup>123</sup> demonstrated the presence of  $h^+$  also played a role in the system apart from  $\bullet OH$  radicals and  $\bullet O_2^-$  radicals. Furthermore, in presence of peroxide, if the composite contains an iron species enhanced generation of  $\bullet OH$  is observed<sup>124</sup>.

Summarizing the discussions, scavenger studies reveal that hydroxyl ( $\bullet OH$ ) radicals and superoxide ( $\bullet O_2^-$ ) radicals are the primary reactive oxygen species while the contribution of valence band holes<sup>215</sup> is dependent on the relative positions of edge gap of the valence band. Notably in many reported systems superoxide radicals behaves as the primary ROS due to efficient electron migration to GO. Therefore, the enhanced photocatalytic efficiency of magnetic MO@GO nanocomposites can be attributed to effective electron trapping,

reduced electron-hole recombination and enhanced radical generation with superoxide radical being the primary ROS.

## 6. Comparison with other catalysts

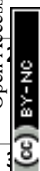
Till date, many heterogeneous photocatalytic systems have been developed for the degradation of organic pollutants. However, magnetically retrievable metal oxide@graphene oxide systems have garnered immense attraction due to their brilliant efficiency, ease of separation, etc. Table 3 lists a comparative data of the parameters associated with the degradation process for different metal oxide based photocatalysts and magnetic metal oxide@graphene oxide-based systems. Even though these nanocomposite systems can be a bit expensive, when compared to unmodified metal oxides they show higher degradation efficiency, similar recovery cycles showcasing stability in aqueous conditions, and in several cases, they can degrade organic pollutants under visible light irradiation, increasing their utility in real world. These characteristics coupled with the ease of separation make them a viable candidate for water remediation *via* degradation of organic pollutants. Despite these advantages, concerns have been raised against the toxicity of the different components of these nanocomposites, therefore the effects of the long-term exposures of these nanocomposites on human health and the environment needs to be further studied.



[Type here]

View Article Online  
DOI: 10.1039/D6VA00059B**Table 3: A critical comparison of photocatalytic activity of unmodified metal oxide photocatalysts and MMO@GO nnanocomposites.**

SNo.	Pollutant class	Photocatalyst	Target Pollutant	Photo Catalyst Separation	Light Source	Degradation Efficiency (%)	Time (in min)	No of recovery Cycles	Ref.	
1	Pharmaceutical	• Antimicrobial	TiO <sub>2</sub> -425	Tetracycline	Centrifugation	UV/Visible	25.1	120	4	216
			ZnO	Ciproflaxin	Filtration	UV	50	60	-	217
			ZnO	Oxytetracycline	Filtration	UV	76.1	80	-	218
		CuFe <sub>2</sub> O <sub>4</sub> /rGO10	Tetracycline	Magnetic separation	Visible	90.44	160	5	128	
		Co <sub>3</sub> O <sub>4</sub> /TiO <sub>2</sub> /GO	Oxytetracycline	Magnetic separation	UV/Visible	91	90	5	126	
		GO@Fe <sub>3</sub> O <sub>4</sub> @TiO <sub>2</sub>	Ciprofloxacin	Magnetic separation	UV/Visible	91.5	240	5	130	
		TiO <sub>2</sub> /Fe <sub>3</sub> O <sub>3</sub> /GO	Metronidazole	Magnetic separation	UV/Visible	97	120	-	121	
		• Psychopharmaceutical	H <sub>2</sub> TiO <sub>7</sub> nanotubes	Clonazepam	Centrifugation	-	80.79	240	4	219
			rGO/TiO <sub>2</sub> /CSA	Caffeine and Carbamazepine	Magnetic separation	UV/Visible	99	60	10	143
			Fe <sub>3</sub> O <sub>4</sub> -graphene oxide	Clonazepam	Magnetic separation	UV	100	5	5	145
	• Antipyretic	TiO <sub>2</sub> P25 rGO/BSO/g-C <sub>3</sub> N <sub>4</sub> Fe <sub>3</sub> O <sub>4</sub> @Mn <sub>3</sub> O <sub>4</sub> -rGO	Paracetamol	Centrifugation	UV	90	150	4	220	
			Naproxen	Filtration	UV	77.52	90	4	221	
			Sulfamethazine	Magnetic separation	UV	98	120	-	134	
	• Estrogen	TiO <sub>2</sub> ZnFe <sub>2</sub> O <sub>4</sub> -Ag/Rgo	Estrone-3-glucuronide	Filtration	UV	25	390	-	222	
			17 $\alpha$ -Ethinylestradiol	Magnetic separation	UV	80	240	5	133	
	• Antidiabetic	TiO <sub>2</sub> -ZrO <sub>2</sub> Fe <sub>3</sub> O <sub>4</sub> @rGO@ZnO/Ag	Metformin	Centrifugation	UV	50	30	-	123	
			Metformin	Magnetic separation	Visible	100	60	5	159	
	Microplastic	GO@metaloxide Fe <sub>3</sub> O <sub>4</sub> @TiO <sub>2</sub> /Ag	Polyethylene	Centrifugation	UV	10.3	480	-	224	
			Polyethylene	Centrifugation	UV	17.54	180	5	225	
	Pesticide	GO-TiO <sub>2</sub> rGO@Fe <sub>3</sub> O <sub>4</sub> @ZnO GO@Fe <sub>3</sub> O <sub>4</sub> @TiO <sub>2</sub> GO@Fe <sub>3</sub> O <sub>4</sub> @CeO <sub>2</sub>	Atrazine	Filtration	UV/Visible	50	59	-	223	
Metalaxyl			Magnetic separation	Visible	92	120	5	116		
Chlorpyrifos			Magnetic separation	Visible	97	60	4	187		
Diazinon			Magnetic separation	Visible	97.9	60	5	189		
4.	Dye	Co <sub>3</sub> O <sub>4</sub> /ZnO	Methylene blue	Centrifugation	-	86	90	-	227	
		ZnO/NiFe <sub>2</sub> O <sub>4</sub>	Methylene blue	-	-	93	70	-	228	
		rGO@Fe <sub>3</sub> O <sub>4</sub> @TiO <sub>2</sub>	Methylene blue	Magnetic separation	Visible	100	5	5	232	
		rGO@Fe <sub>3</sub> O <sub>4</sub> @V <sub>2</sub> O <sub>5</sub>	Acid Orange 7	Magnetic separation	Visible	93.3	70	5	85	
		rGO@Fe <sub>3</sub> O <sub>4</sub> @V <sub>2</sub> O <sub>5</sub>	Bismarck Brown	Magnetic separation	Visible	94.3	70	5	85	



## 7. Challenges, Future Research, Directions and SWOT Analysis of Metal Oxide @Graphene Oxide Nanocomposites

Magnetic MMO nanocomposites represent a promising class of engineered materials with wide ranging applications in catalysis, energy storage, environmental remediation and sensing technologies. However, despite their immense potential, the transition from laboratory-scale to large scale operations presents a new set of scientific, technological, and environmental challenges. In this regard, a systematic SWOT (Strengths, Weaknesses, Opportunities Threats) analysis becomes essential to highlight the current state and future trajectory of these nanocomposites.

The primary strengths of these nanocomposites lie in their multifunctional characteristics, which include improved magnetic, tunable electronic properties, large surface area, high efficiency, thermal and chemical stability, reusability and mechanical robustness<sup>25,26,229-231</sup>. Despite these advantages, significant weaknesses require considerable attention. The most critical challenge is the lack of scalable, reproducible, and environmentally benign synthesis methods. Many current strategies involve complex, multi-step processes involving toxic reagents or harsh conditions, which are incompatible with large-scale manufacturing<sup>232</sup>. Homogeneous dispersion of metal oxide nanoparticles on the GO sheets is difficult to achieve due to aggregation of MO. This directly impacts the performance consistency of the resulting photocatalyst<sup>233</sup>. Another fundamental weakness is the charge recombination which although mitigated by GO, still appears, especially in composites with suboptimal interfacial contact or excessive GO loading that can shield active sites<sup>229</sup>. Additionally, studies regarding the long-term structural stability and catalyst recyclability under various conditions (e.g. in aqueous environments of varying matrix composition or pH or at different temperatures) are often limited. Nanoparticles can leach out and the GO support may degrade over multiple cycles under diverse conditions leading to performance decay<sup>234</sup>.

These weaknesses point directly to key opportunities for future research. There is a need for the development of green, one pot synthesis strategies that are energy-efficient, use water as a solvent and avoid hazardous chemicals. These include methods such as hydrothermal, solvothermal, or mechanochemical based synthesis<sup>235,236</sup>. Research should focus on engineering the MMO-GO interface at the atomic level to maximize charge transfer efficiency and minimize recombination losses. This may include covalent functionalization or the creation of heterojunctions with tailored band alignments. Another major opportunity lies in designing hierarchical or 3D architectures (e.g., aerogels, foams) that can prevent restacking of GO sheets

while maintaining high surface area, facilitating mass transport<sup>237</sup>. Furthermore, integrating MMO@GO composites into practical devices, such as flow reactors for water treatment represents an important step toward real-world application<sup>238</sup>. However, these opportunities are associated with serious threats that need to be addressed.

The foremost threat is the potential environmental and health impact of these nanomaterials. The long-term ecotoxicity of these nanocomposites, their persistence in ecosystems, and their potential to bioaccumulate are not yet fully understood<sup>239</sup>. Without comprehensive life-cycle assessments and clear regulatory frameworks, public and governmental acceptance represents a significant barrier. Another threat is the economic viability of large-scale production. High cost of superior quality GO and complexity of controlled synthesis may render these materials too expensive for many applications compared to conventional materials.

While MMO@GO nanocomposites possess a remarkable set of strengths that makes them ideal candidates for next-generation technologies, their real-world applications depend upon overcoming substantial weaknesses in synthesis and stability. Through innovation in green manufacturing and advanced architecture design while actively addressing the threats related to environmental safety and economic feasibility, the full potential of these materials can be harnessed. Future research must adopt a holistic, interdisciplinary approach encompassing materials chemistry, process engineering, and environmental science to ensure their sustainable and responsible development.

## 8. Conclusions

The evolution of nanocomposites based on the integration of magnetic compounds such as oxides and ferrites into graphene oxide nanosheets along with metal oxides, is a transformative approach towards the sustainable photocatalytic degradation of organic pollutants in aqueous media. By leveraging the high surface area, electron mobility, and functional versatility of graphene oxide with the redox activity and UV and visible-light responsiveness of engineered metal oxides, such systems offer enhanced charge separation, prolonged catalyst lifetime, and superior degradation efficiencies. In this review, we have discussed the various methods for the synthesis of magnetically retrievable metal oxide/graphene oxide and metal oxide/reduced graphene oxide nanocomposites, their application as photocatalysts in the degradation of pharmaceuticals, microplastics, pesticides and dyes in aqueous media, and their role in various organic transformations. The synergistic integration of metal oxides, graphene oxide, and



[Type here]

ferrite nanoparticles in nanocomposite systems plays a crucial role in enhancing catalytic activity and improving pollutant removal efficiency. The literature reviewed in this study demonstrates that these composite materials exhibit remarkable degradation performance, often achieving up to 100% pollutant removal within a short reaction time under optimized conditions. Moreover, their excellent stability and reusability, with minimal loss of catalytic activity over multiple cycles, make them highly promising candidates for sustainable water treatment technologies. Therefore, such integrated nanocomposite systems represent a significant advancement in the field of environmental remediation and offer strong potential for future development in efficient and cost-effective wastewater treatment applications.

### Author contributions

AS, SD, RKS and RJ were involved in the conceptualization, and design of the work. SD, PK, Kirti, RS and Priyanka contributed in reviewing and editing the manuscript. Kirti, VKU, Geetanshu and SNK were involved in the literature review, data curation and writing of the manuscript.

### Conflicts of interest

There are no conflicts to declare.

### Data availability

All data discussed in this review are drawn from previously published sources, which are cited in the reference list.

### Acknowledgements

Kirti would like to thank CSIR for the award of Senior Research Fellowship. SD would like to thank Hindu College for the award of Lalit Kumar Jain Memorial Research Fellowship.

### References

- 1 N. Morin-Crini, E. Lichtfouse, G. Liu, V. Balaram, A. R. L. Ribeiro, Z. Lu, F. Stock, E. Carmona, M. R. Teixeira, L. A. Picos-Corrales, J. C. Moreno-Piraján, L. Giraldo, C. Li, A. Pandey, D. Hocquet, G. Torri and G. Crini, *Environmental Chemistry Letters*, 2022, 20, 2311–2338.
- 2 L. Lin, H. Yang and X. Xu, *Frontiers in Environmental Science*, 2022, Volume 10 - 2022.
- 3 R. Fuller, P. J. Landrigan, K. Balakrishnan, G. Bathan, S. Bose-O'Reilly, M. Brauer, J. Caravanos, T. Chiles, A. Cohen, L. Corra, M. Cropper, G. Ferraro, J. Hanna, D. Hanrahan, H. Hu, D. Hunter, G. Janata, R. Kupka, B. Lanphear, M. Lichtveld, K. Martin, A. Mustapha, E. Sanchez-Triana, K. Sandilya, L. Schaeffli, J. Shaw, J. Seddon, W. Suk, M. M. Téllez-Rojo and C. Yan, *Lancet Planet Health*, 2022, 6, e535–e547.

- 4 A. Mandal, P. Senthil Kumar, C. S. Poorva, L. Srinivasa Raju, S. R. Balasubramani and G. Rangasamy, *Water Practice and Technology*, 2024, 19, 937–959.
- 5 K. C. Jones and P. de Voogt, *Environmental Pollution*, 1999, 100, 209–221.
- 6 M. A. Ashraf, *Environmental Science and Pollution Research*, 2017, 24, 4223–4227.
- 7 A. B. T. Akhtar, S. Naseem, A. Yasar and Z. Naseem, in *Environmental pollution and remediation*, Springer, 2021, pp. 213–246.
- 8 W. A. H. Altowayti, S. Shahir, N. Othman, T. A. E. Eisa, W. M. S. Yafooz, A. Al-Dhaqm, C. Y. Soon, I. B. Yahya, N. A. N. b. Che Rahim, M. Abaker and A. Ali, *Processes*, 2022, 10, 1832.
- 9 A. T. Nguyen and L. Le Tran, *Reviews of Environmental Contamination and Toxicology*, 2024, 262, 11.
- 10 A. Al Miad, S. P. Saikat, M. K. Alam, M. S. Hossain, N. M. Bahadur and S. Ahmed, *Nanoscale Adv.*, 2024, 6, 4781–4803.
- 11 X. Zhang, Y. L. Chen, R. S. Liu and D. P. Tsai, *Rep Prog Phys*, 2013, 76, 046401.
- 12 R. Schlögl and S. B. Abd Hamid, *Angewandte Chemie International Edition*, 2004, 43, 1628–1637.
- 13 P. Christopher, D. B. Ingram and S. Lincic, *The Journal of Physical Chemistry C*, 2010, 114, 9173–9177.
- 14 L. L. Zhang, Z. Xiong and X. S. Zhao, *ACS Nano*, 2010, 4, 7030–7036.
- 15 G. Williams, B. Seger and P. V. Kamat, *ACS Nano*, 2008, 2, 1487–1491.
- 16 K. C. Kemp, H. Seema, M. Saleh, N. H. Le, K. Mahesh, V. Chandra and K. S. Kim, *Nanoscale*, 2013, 5, 3149–3171.
- 17 F. T. Geldasa, M. A. Kebede, M. W. Shura and F. G. Hone, *RSC Adv.*, 2023, 13, 18404–18442.
- 18 T. Velempini, E. Prabakaran and K. Pillay, *Mater. Today Chem.*, 2021, 19, 100380.
- 19 K. H. Kumar, H. T. Ananda, D. K. Ravishankar, H. Madhu and S. Thirumala, *Sustainable Chem. One World*, 2025, 100055.
- 20 X. Hong, X. Wang, Y. Li, J. Fu and B. Liang, *Catalysts*, 2020, 10, 921.
- 21 K. Q. Lu, Y. H. Li, Z. R. Tang and Y. J. Xu, *ACS Mater. Au*, 2021, 1, 37–54.
- 22 C. Rios, L. Bazán-Díaz, C. A. Celaya, R. Salcedo and P. Thangarasu, *Molecules*, 2023, 28, 7331.
- 23 Y. Feng, X. Su, Y. Chen, Y. Liu, X. Zhao, C. Lu, Y. Ma, G. Lu and M. Ma, *Materials Research Bulletin*, 2023, 162, 112207.
- 24 A. Singh, D. Singh, B. Ahmed, Animesh K. Ojha, *Materials Chemistry and Physics*, 277, 2022, 125531, 0254-0584
- 25 P. Majumder and R. Gangopadhyay, *RSC Advances*, 2022, 12, 5686–5719.
- 26 N. Mushahary, A. Sarkar, F. Basumatary, S. Brahma, B. Das and S. Basumatary, *Results in Surfaces and Interfaces*, 2024, 15, 100225.
- 27 M. Zubair, R. Syamaladevi and A. Ullah, *Environmental Science: Nano*, 2024.
- 28 S. K. Sharma and S. Sharma, *Chemical Engineering & Technology*, 2025, 48, e70009.
- 29 B. Anegebe, I. H. Ifijen, M. Maliki, I. E. Uwidia and A. I. Aigbodion, *Environmental Sciences Europe*, 2024, 36.
- 30 Y. Wei, G. Duan, Y. Huang, X. Han, C. Zhang, S. He, H. Zhao, C. Ma and S. Jiang, *Journal of Water Process Engineering*, 2025, 74, 107766.
- 31 M. U. Farooq and M. I. Jalees, *Journal of Water Process Engineering*, 2020, 33, 101044.
- 32 B. Bhushan, P. Negi, A. Nayak and S. Goyal, *Advanced Composites and Hybrid Materials*, 2024, 8, 55.
- 33 S. Abbasi, *Applied Water Science*, 2023, 13, 128.
- 34 Rajendrakumar, S., Mavhaire, D., Shimly, S., Tharanidevi, N., Ramachandran, V. S., & Timilsina, R. R. (2025). Drivers and barriers towards achieving SDG 6 on clean water and



- sanitation for all-an Indian perspective. *World Development Sustainability*, 7, 100228.
- 35 Singh, S., & Jayaram, R. (2022). Attainment of water and sanitation goals: a review and agenda for research. *Sustainable water resources management*, 8(5), 146–3
- 36 M. Nikazar, M. Alizadeh, R. Lalavi and M. H. Rostami, *J Environ Health Sci Eng*, 2014, 12, 21.
- 37 W. S. Hummers, Jr. and R. E. Offeman, *Journal of the American Chemical Society*, 1958, 80, 1339–1339
- 38 D. C. Marcano, D. V. Kosynkin, J. M. Berlin, A. Sinitskii, Z. Sun, A. Slesarev, L. B. Alemany, W. Lu and J. M. Tour, *ACS Nano*, 2010, 4, 4806–4814.
- 39 S. Abbasi, F. Ahmadpoor, M. Imani and M.-S. EkramiKakhki, *International Journal of Environmental Analytical Chemistry*, 2020, 100, 225–240.
- 40 R. Eivazzadeh-Keihan, R. Taheri-Ledari, N. Khosropour, S. Dalvand, A. Maleki, S. M. Mousavi-Khoshdel and H. Sohrabi, *Colloids and Surfaces A: Physicochemical and Engineering Aspects*, 2020, 587, 124335.
- 41 A. Bateni, K. Valizadeh, Y. Salahshour, A. H. Behrooz and A. Maleki, *Journal of Environmental Management*, 2022, 324, 116358.
- 42 N. Salimi, E. Mohammadi-Manesh, N. Ahmadvand, H. Danafar and S. Ghiasvand, *Journal of Inorganic and Organometallic Polymers and Materials*, 2024, 34, 1256–1271.
- 43 C. B. Anucha, I. Altin, E. Bacaksiz and V. N. Stathopoulos, *Chemical Engineering Journal Advances*, 2022, 10, 100262.
- 44 K. Nakata and A. Fujishima, *J. Photochem. Photobiol. C: Photochem. Rev.*, 2012, 13, 169–189.
- 45 M. Cao, P. Wang, Y. Ao, C. Wang, J. Hou and J. Qian, *Chemical Engineering Journal*, 2015, 264, 113–124.
- 46 P. Wang, Y. Ao, C. Wang, J. Hou and J. Qian, *Carbon*, 2012, 50, 5256–5264.
- 47 Z. Li, F. Chen, L. Yuan, Y. Liu, Y. Zhao, Z. Chai and W. Shi, *Chemical Engineering Journal*, 2012, 210, 539–546.
- 48 Z.-J. Li, Z.-W. Huang, W.-L. Guo, L. Wang, L.-R. Zheng, Z.-F. Chai and W.-Q. Shi, *Environmental science & technology*, 2017, 51, 5666–5674.
- 49 Y. Liang, H. Wang, H. Sanchez Casalongue, Z. Chen and H. Dai, *Nano Research*, 2010, 3, 701–705.
- 50 B. K. Ghosh, D. Moitra, M. Chandel and N. N. Ghosh, *Journal of Nanoscience and Nanotechnology*, 2017, 17, 4694–4703.
- 51 Q. Li, H. Kong, P. Li, J. Shao and Y. He, *Journal of hazardous materials*, 2019, 373, 437–446.
- 52 J. Mehralipour, S. Bagheri and M. Gholami, *Heliyon*, 2023, 9
- 53 D. Bala, I. Matei, G. Ionita, D.-V. Cosma, M.-C. Rosu, M. Stanca, C. Gaidau, M. Baleanu, M. Virgolici and I. Stanculescu, *International Journal of Molecular Sciences*, 2022, 23, 14703.
- 54 D. Cosma, A. Urda, T. Radu, M. C. Rosu, M. Mihet and C. Socaci, *Molecules*, 2022, 27, 5803.
- 55 F. Pogacean, C. Socaci, S. Pruneanu, A. R. Biris, M. Coros, L. Magerusan, G. Katona, R. Turcu and G. Borodi, *Sensors and Actuators B: Chemical*, 2015, 213, 474–483.
- 56 A. Pelella, O. Kharsah, A. Grillo, F. Urban, M. Passacantando, F. Giubileo, L. Lemmo, S. Sleziona, E. Pollmann and L. Madauß, *ACS applied materials & interfaces*, 2020, 12, 40532–40540.
- 57 A. Pelella, A. Grillo, F. Urban, F. Giubileo, M. Passacantando, E. Pollmann, S. Sleziona, M. Schleberger and A. Di Bartolomeo, *Advanced Electronic Materials*, 2021, 7, 2000838.
- 58 X. Zhang, P. Yu, Y. Chen and Y. Ma, *Materials Letters*, 2010, 64, 583–585. View Article Online  
DOI: 10.1039/D6VA00059B
- 59 D. Liu, B. B. Garcia, Q. Zhang, Q. Guo, Y. Zhang, S. Sepehri and G. Cao, *Advanced Functional Materials*, 2009, 19, 1015–1023.
- 60 M. Zhou, X. Zhang, J. Wei, S. Zhao, L. Wang and B. Feng, *The Journal of Physical Chemistry C*, 2011, 115, 1398–1402.
- 61 L. Zhang, J. Lian, L. Wu, Z. Duan, J. Jiang and L. Zhao, *Langmuir*, 2014, 30, 7006–7013.
- 62 X. Chen, Y.-F. Shen, S. L. Suib and C. B. Zhi, H. Ding, D. Wang, Y. Cao, Y. Zhang, X. Wang, Y. Liu and Q. Huo, *Journal of Materials Chemistry A*, 2014, 2, 2374–2382.
- 63 B. Zhi, H. Ding, D. Wang, Y. Cao, Y. Zhang, X. Wang, Y. Liu and Q. Huo, *Journal of Materials Chemistry A*, 2014, 2, 2374–2382.
- 64 Q. Tang, M. Sun, S. Yu and G. Wang, *Electrochimica Acta*, 2014, 125, 488–496.
- 65 J. Tang, M. Myers, K. A. Bosnick and L. E. Brus, *The Journal of Physical Chemistry B*, 2003, 107, 7501–7506.
- 66 Y. Liu, C. Luo, G. Cui and S. Yan, *RSC Advances*, 2015, 5, 54156–54164.
- 67 L. Tan, J. Wang, Q. Liu, Y. Sun, X. Jing, L. Liu, J. Liu and D. Song, *New Journal of Chemistry*, 2015, 39, 868–876.
- 68 J. Li, Y. Chen, Q. Wu and H. Xu, *Journal of Alloys and Compounds*, 2017, 693, 373–380
- 69 B. M. Weckhuysen and D. E. Keller, *Catalysis Today*, 2003, 78, 25–46.
- 70 M. Shanmugam, A. Alsalmeh, A. Alghamdi and R. Jayavel, *ACS applied materials & interfaces*, 2015, 7, 14905–14911.
- 71 P. K. Boruah, S. Szunerits, R. Boukherroub and M. R. Das, *Chemosphere*, 2018, 191, 503–513.
- 72 F. Jafari and F. R. Rahsepar, *ACS omega*, 2023, 8, 35427–35439.
- 73 W. M. Husain, J. K. Araak and O. M. Ibrahim, *The Iraqi Journal of Veterinary Medicine*, 2019, 43, 6–14.
- 74 R. A. Salman, *Ibn AL-Haitham Journal For Pure and Applied Science*, 2018, 31, 9–14.
- 75 A. J. Katafa and M. K. Hamid, *Iraqi Journal of Science*, 2020, 540–549.
- 76 N. J. Hattab, E. E. Laibi and M. M. Mohammed, *Ibn ALHaitham Journal For Pure and Applied Sciences*, 2024, 37, 316–332.
- 77 A. F. Abdalzhra, I. A. Abdllatif and E. E. L. Alabodi, *Ibn ALHaitham Journal For Pure and Applied Science*, 2016, 29, 379–389.
- 78 N. Horti, M. Kamatagi, S. Nataraj, M. Sannaikar and S. Inamdar, 2020.
- 79 R. Chintaparty, B. Palagiri, R. R. Nagireddy and V. S. R. I. Reddy, *Phase Transitions*, 2015, 88, 929–938.
- 80 J. Park, J. C. Hwang, G. G. Kim and J. U. Park, *InfoMat*, 2020, 2, 33–56.
- 81 J. K. Patel, A. Patel and D. Bhatia, in *Emerging technologies for nanoparticle manufacturing*, Springer, 2021, pp. 3–23.
- 82 N. M. El-Shafai, M. E. El-Khouly, M. El-Kemary, M. S. Ramadan and M. S. Masoud, *RSC advances*, 2018, 8, 13323–13332.
- 83 A.F. Ismail and E. E. Al Abodi, *Advanced Journal of Chemistry*, 2025, 8(3), 615–627
- 84 S. Todorova, J.-L. Cao, D. Paneva, K. Tenchev, I. Mitov, G. Kadinov, Z.-Y. Yuan and V. Idakiev, in *Studies in surface science and catalysis*, Elsevier, 2010, vol. 175, pp. 547–550.
- 85 N. Ghassemi, S. S. H. Davarani and H. R. Moazami, *Journal of Materials Science: Materials in Electronics*, 2018, 29, 12573–12583.



[Type here]

- 86 V. A. Tran, T. L. H. Nguyen and V.-D. Doan, *Chemosphere*, 2021, 270, 129417.
- 87 K. H. P. Ngoc and A.-T. Vu, *Adsorption Science & Technology*, 2022, 2022, 6454354.
- 88 P. Xu, P. Wang, X. Li, R. Wei, X. Wang, C. Yang, T. Shen, T. Zheng and G. Zhang, *Chemical Engineering Journal*, 2022, 440, 135863.
- 89 Y. Jain, M. Kumari, R. P. Singh, D. Kumar and R. Gupta, *Catalysis Letters*, 2020, 150, 1142–1154.
- 90 N. Nasseh, F. S. Arghavan, N. Daglioglu and A. Asadi, *Environmental Science and Pollution Research*, 2021, 28, 19222–19233.
- 91 A. Di Bartolomeo, L. Lemmo, F. Giubileo, G. Luongo, F. Urban and A. Grillo, 2018.
- 92 W. Fu, X. Xu, W. Wang, J. Shen and M. Ye, *ACS Sustainable Chemistry & Engineering*, 2018, 6, 8935–8944.
- 93 M. Park, Y. J. Park, X. Chen, Y. K. Park, M. S. Kim and J. H. Ahn, *Advanced Materials*, 2016, 28, 2556–2562.
- 94 Yan, Z. Chen, H. Ji, Z. Liu, X. Wang, Y. Xu, X. She, L. Huang, L. Xu and H. Xu, *Chemistry—A European Journal*, 2016, 22, 4764–4773.
- 95 S. Zhang, R. Hu, P. Dai, X. Yu, Z. Ding, M. Wu, G. Li, Y. Ma and C. Tu, *Applied Surface Science*, 2017, 396, 994–999.
- 96 W. Yin, L. Yan, J. Yu, G. Tian, L. Zhou, X. Zheng, X. Zhang, Y. Yong, J. Li and Z. Gu, *ACS nano*, 2014, 8, 6922–6933.
- 97 W. Zhou, Y. Zhang, Y. Li, Y. Gou and X. Zhou, *Ceramics International*, 2022, 48, 1908–1915.
- 98 X. Han, Y. Huang, J. Wang, X. Du, L. Hu, T. Li and X. Sun, *Composites Part B: Engineering*, 2022, 239, 109965.
- 99 N. Liu, Y. Dou, X. Zhang, L. Yu and X. Yan, *Carbon*, 2022, 190, 125–135.
- 100 D. Mu, Z. Chen, H. Shi and N. Tan, *RSC advances*, 2018, 8, 36625–36631.
- 101 S. Tajik, A. A. Afshar, S. Shamsadini, M. B. Askari, Z. Dourandish, F. Garkani Nejad, H. Beitollahi and A. Di Bartolomeo, *Industrial & Engineering Chemistry Research*, 2022, 62, 4473–4480.
- 102 X. Ding, G. Fan, Y. Huang and J. Wang, *Journal of Materials Science: Materials in Electronics*, 2021, 32, 9640–9649.
- 103 Z. Wang, 3-D flower-like (MoS<sub>2</sub>/Fe<sub>3</sub>O<sub>4</sub>)@rGO composite with multi-level structures for enhanced microwave absorption performance, *SSRN*, 2022, 4217615
- 104 S. Cherukulappurath and S. R. Amonkar, *Available at SSRN 5054731*.
- 105 F. Soltani-nezhad, A. Saljooqi, T. Shamspur and A. Mostafavi, *Polyhedron*, 2019, 165, 188–196.
- 106 V. K. Gupta, T. Eren, N. Atar, M. L. Yola, C. Parlak and H. Karimi-Maleh, *Journal of Molecular Liquids*, 2015, 208, 122–129.
- 107 P. K. Boruah, S. Szunerits, R. Boukherroub and M. R. Das, *Chemosphere*, 2018, 191, 503–513.
- 108 T. L. Lemke, D. A. Williams, V. F. Roche and S. W. Zito, *Foye's Principles of Medicinal Chemistry: Seventh Edition*, 2013.
- 109 M. Aitken, M. Kleinrock and J. Pritchett, *Global Use of Medicines 2024*, 2024.
- 110 A. C. Duarte, S. Rodrigues, A. Afonso, A. Nogueira and P. Coutinho, *Pharmaceuticals (Basel)*, 2022, 15.
- 111 S. K. Srivastava, *RSC Applied Interfaces*, 2024, 1, 340–429.
- 112 K. Samal, S. Mahapatra and M. Hibzur Ali, *Energy Nexus*, 2022, 6, 100076.
- 113 A. O. Oluwole and O. S. Olatunji, *Environmental Sciences Europe*, 2022, 34, 5.
- 114 M. Patel, R. Kumar, K. Kishor, T. Mlsna, C. U. Pittman, Jr. and D. Mohan, *Chem Rev*, 2019, 119, 3510–3673.
- 115 D. Papagiannaki, M. H. Belay, N. P. Goncalves, E. Robotti, A. Bianco-Prevot, R. Binetti and P. Calza, *Chemical Engineering Journal Advances*, 2022, 10, 100245.
- 116 B. S. Rathi, P. S. Kumar and D. N. Vo, *Sci Total Environ*, 2021, 797, 149134.
- 117 J. Kusi, C. O. Ojewole, A. E. Ojewole and I. Nwi-Mozu, *Antibiotics (Basel)*, 2022, 11.
- 118 M. Antonopoulou, C. Kosma, T. Albanis and I. Konstantinou, *Science of The Total Environment*, 2021, 765, 144163.
- 119 Emmanuel, S. S., Alanazi, A. K., Adesibikan, A. A., Olawoyin, C. O., Abimbola, E. T., & Oluwole, O. J. (2025). Graphene/graphitic-based metal-organic frameworks (MOFs) for photocatalytic degradation of pharmaceutical pollutants: A review. *Journal of Organometallic Chemistry*, 123915.
- 120 C. Du, Z. Zhang, S. Tan, G. Yu, H. Chen, L. Zhou, L. Yu, Y. Su, Y. Zhang, F. Deng and S. Wang, *Environmental Research*, 2021, 200, 111427.
- 121 C. Aruljothi, P. Balaji, E. Vaishnavi, T. Pazhanivel and T. Vasuki, *Journal of Chemical Technology & Biotechnology*, 2023, 98, 1908–1917P.
- 122 D. Qiao, Z. Li, J. Duan and X. He, *Chemical Engineering Journal*, 2020, 400, 125952.
- 123 Barathe, K. Kaur, S. Reddy, V. Shriram and V. Kumar, *Journal of Hazardous Materials Letters*, 2024, 5, 100105.
- 124 W. Shi, L. Wang, J. Wang, H. Sun, Y. Shi, F. Guo and C. Lu, *Separation and Purification Technology*, 2022, 292, 120987.
- 125 W.-K. Jo, S. Kumar, M. A. Isaacs, A. F. Lee and S. Karthikeyan, *Applied Catalysis B: Environmental*, 2017, 201, 159–168.
- 126 Sekar, Karthikeyan & Jo, Wan & Kumar, Santosh & Isaacs, Mark & Lee, Adam. (2016). Cobalt promoted TiO<sub>2</sub>/GO for the photocatalytic degradation of oxytetracycline and Congo Red. *Applied Catalysis B Environmental*. 201. 159-168. 10.1016/j.apcatb.2016.08.022.
- 127 W. Anku, E. Kiarri, R. Sharma, G. Joshi, S. Shukla and P. Govender, 2019, DOI: 10.1007/978-3-319-75484-0\_7, pp. 187–208.
- 128 D. T. Sponza, & Koyuncuoglu, P., *Clinical Microbiology and Infectious Diseases*, 2019, 4.
- 129 S. Uruş, M. Çaylar, H. Eskalen and Ş. Özgan, *Journal of Materials Science: Materials in Electronics*, 2022, 33, 4314–4329.
- 130 M. Farhadian, N. Entezami and N. Davari, *Advances in environmental science and technology*, 2019, 5, 55–65.
- 131 J. " Wu J, Bai J, Wang Z, Liu Z, Mao Y, Liu B, Zhu X. UV-assisted nitrogen-doped reduced graphene oxide/Fe<sub>3</sub>O<sub>4</sub> composite activated peroxodisulfate degradation of norfloxacin. *Environ Technol*. 2022 Jan;43(1):95-106
- 132 B. Kakavandi, E. Dehghanifard, P. Gholami, M. Noorisepehr and B. MirzaHedayat, *Applied Surface Science*, 2021, 570, 151145.
- 133 Z. Wan and J. Wang, *Journal of Hazardous Materials*, 2017, 324, 653–664.
- 134 L. Chen, J. Peng, F. Wang, D. Liu, W. Ma, J. Zhang, W. Hu, N. Li, P. Dramou and H. He, *Environ Sci Pollut Res Int*, 2021, 28, 21799–21811
- 135 R. Nimshi, J. Vijaya, L. Kennedy, S. Selvamani P, M. Bououdina and P. Sophia, *Ceramics International*, 2022, DOI: 10.1016/j.ceramint.2022.12.254.
- 136 Y. Zhu, J. Xue, T. Xu, G. He and H. Chen, *Journal of Materials Science: Materials in Electronics*, 2017, 28, 1–10.
- 137 D. Sharma, H. Kumar and S. Kumar, *Applied Materials Today*, 2025, 44, 102706.
- 138 D. M. Aronoff and E. G. Neilson, *Am. J. Med.*, 2001, 111, 304–315.

View Article Online

DOI: 10.1039/C4PY00958E



- 139 G. S. Lipman, F. G. Gaudio, K. P. Eifling, M. A. Ellis, E. M. Otten and C. K. Grissom, *Wilderness & Environmental Medicine*, 2019, **30**, S33–S46.
- 140 F. J. Enguita, S. Pereira and A. L. Leitão, *J Fungi (Basel)*, 2023, **9**.
- 141 N. Dwivedi and S. Dwivedi, *Bionanotechnology Towards Sustainable Management of Environmental Pollution*, 2022.
- 142 J. Chen, Q. Zhang, W. Chen, U. Farooq, T. Lu, B. Wang, J. Ni, H. Zhang and Z. Qi, *Environmental Science: Processes & Impacts*, 2023, **25**, 2092–2101.
- 143 R. Santhosh Kumar, K. Govindan, S. Ramakrishnan, A. R. Kim, J.-S. Kim and D. J. Yoo, *Applied Surface Science*, 2021, **556**, 149765.
- 144 A. Castellano-Hinojosa, M. J. Gallardo-Altamirano, J. González-López and A. González-Martínez, *J Hazard Mater*, 2023, **447**, 130818.
- 145 N. Rashtchi, S. Sobhanardakani, M. Cheraghi, A. Goodarzi and B. Lorestani, *Toxin Reviews*, 2023, **42**, 701–708.
- 146 C. J. E. Davey, M. H. S. Kraak, A. Praetorius, T. L. Ter Laak and A. P. van Wezel, *Water Res*, 2022, **222**, 118878.
- 147 S. Linley, Y. Liu, C. J. Ptacek, D. W. Blowes and F. X. Gu, *ACS Applied Materials & Interfaces*, 2014, **6**, 4658–4668.
- 148 M. P. da Silva, A. C. A. de Souza, Á. R. D. Ferreira, P. L. A. do Nascimento, T. J. M. Fraga, J. V. F. L. Cavalcanti, M. G. Ghislandi and M. A. da Motta Sobrinho, *Scientific Reports*, 2024, **14**, 18916.
- 149 M. Moztahida, J. Jang, M. Nawaz, S.-R. Lim and D. S. Lee, *Science of The Total Environment*, 2019, **667**, 741–750.
- 150 K. Sornalingam, A. McDonagh and J. L. Zhou, *Sci Total Environ*, 2016, **550**, 209–224.
- 151 E. R. Kabir, M. S. Rahman and I. Rahman, *Environmental toxicology and pharmacology*, 2015, **40**, 241–258.
- 152 Y. Sun, H. Huang, Y. Sun, C. Wang, X.-L. Shi, H.-Y. Hu, T. Kameya and K. Fujie, *Environmental Pollution*, 2013, **180**, 339–344.
- 153 A. A. Bayode, S. S. Emmanuel, S. O. Sanni, O. A. Olalekan, O. T. Ore, D. T. Koko and M. O. Omorogie, *Environmental Chemistry and Ecotoxicology*, 2024, **6**, 315–337.
- 154 N. Khadgi, Y. Li, A. R. Upreti, C. Zhang, W. Zhang, Y. Wang and D. Wang, *Photochemistry and Photobiology*, 2016, **92**, 238–246.
- 155 J. M. Thomas, *Journal*, 2012, 468, 1884–1903.
- 156 C. Trautwein, J. D. Berset, H. Wolschke and K. Kümmerer, *Environ Int*, 2014, **70**, 203–212.
- 157 A. Balakrishnan, M. Sillanpää, M. M. Jacob and D. N. Vo, *Environ Res*, 2022, **213**, 113613.
- 158 A. H. Cheshme Khavar, G. Moussavi, A. Mahjoub, K. Yaghmaeian, V. Srivastava, M. Sillanpää and M. Satari, *Catalysis Science & Technology*, 2019, **9**, 5819–5837.
- 159 Z. Akdogan and B. Guven, *Environmental Pollution*, 2019, **254**, 113011.
- 160 H. Kye, J. Kim, S. Ju, J. Lee, C. Lim and Y. Yoon, *Heliyon*, 2023, **9**, e14359.
- 161 A. Ashrafy, A. A. Liza, M. N. Islam, M. M. Billah, S. T. Arafat, M. M. Rahman and S. M. Rahman, *Journal of Hazardous Materials Advances*, 2023, **9**, 100215.
- 162 I. B. Cooper, K.A., Sinclair, C.R. and Watson, D.H., Eds., *Chemical Migration and Food Contact Materials*, Elsevier, 2007, 228–250.
- 163 E. Marcharla, S. Vinayagam, L. Gnanasekaran, M. Soto-Moscoso, W.-H. Chen, S. Thanigaivel, and S. Ganesan, *Environmental Research*, 2024, **256**, 119181. DOI: 10.1016/j.envres.2024.119181
- 164 L. Jia, L. Liu, Y. Zhang, W. Fu, X. Liu, Q. Wang, M. Tanveer and L. Huang, *Front Plant Sci*, 2023, **14**, 1226484.
- 165 M. Sajjad, Q. Huang, S. Khan, M. A. Khan, Y. Liu, J. Wang, F. Lian, Q. Wang and G. Guo, *Environmental Technology & Innovation*, 2022, **27**, 102408.
- 166 A. Bhowmik, G. Saha and S. C. Saha, *Pollutants*, 2024, **4**, 490–497.
- 167 Y. Li, L. Tao, Q. Wang, F. Wang, G. Li and M. Song, *Environment & Health*, 2023, **1**, 249–257.
- 168 K. Ziani, C. B. Ioniță-Mîndrican, M. Mititelu, S. M. Neacșu, C. Negrei, E. Moroșan, D. Drăgănescu and O. T. Preda, *Nutrients*, 2023, **15**.
- 169 L.-C. Wang, J. C.-T. Lin, J.-A. Ye, Y. C. Lim, C.-W. Chen, C.-D. Dong and T.-K. Liu, *Environmental Science & Technology*, 2024, **58**, 22391–22404.
- 170 C. Ompala, J. P. Renault, O. Taché, É. Cournède, S. Devineau and C. Chivas-Joly, *J Hazard Mater*, 2024, **469**, 134083.
- 171 Z. Chen, X. Liu, W. Wei, H. Chen and B.-J. Ni, *Water Research*, 2022, **221**, 118820.
- 172 J. Talvitie, A. Mikola, A. Koistinen and O. Setälä, *Water Research*, 2017, **123**, 401–407.
- 173 A. Abdelrasoul and H. Westphalen, in *Water Challenges of an Urbanizing World*, ed. M. Glavan, IntechOpen, Rijeka, 2017, DOI: 10.5772/intechopen.71494.
- 174 E. Yousif and R. Haddad, *Springerplus*, 2013, **2**, 398.
- 175 R. Verma, S. Singh, M. K. Dalai, M. Saravanan, V. V. Agrawal and A. K. Srivastava, *Materials & Design*, 2017, **133**, 10–18.
- 176 V. UshaVipinachandran, N. K, K. H. B. Haroon, I. Ashokan, A. Sinha, P. Maity and S. K. Bhunia, *Advanced Sustainable Systems*, n/a, 2500096.
- 177 P. Devi, A. Soni and J. P. Singh, *Journal of Polymer Research*, 2024, **31**, 152.
- 178 I. Uogintė, S. Pleskytė, M. Skapas, S. Stanionytė and G. Lujanienė, *International Journal of Environmental Science and Technology*, 2023, **20**, 9693–9706.
- 179 R. Kumar, *Advanced Sustainable Systems*, 2023, **7**, 2300033.
- 180 *Emerging Materials for Photodegradation and Environmental Remediation of Micro- and Nano-Plastics: recent developments and future prospects*, ed. L. Singh and S. Kumar, 2025, pp. 281–300.
- 181 I. Mahmood, S. R. Imadi, K. Shazadi, A. Gul and K. R. Hakeem, *Plant, Soil and Microbes: Volume 1: Implications in Crop Science*, Springer International Publishing, Cham, 2016, pp. 253–269.
- 182 M. H. Hashimi, R. Hashimi and Q. Ryan, *Asian Plant Res. J.*, 2020, **5**, 37–47.
- 183 G. Luna-Sanguino, A. Ruiz-Delgado, A. Tolosana-Moranchel, L. Pascual, S. Malato, A. Bahamonde and M. Faraldos, *Sci. Total Environ.*, 2020, **737**, 140286.
- 184 T. S. Natarajan, P. K. Gopi, K. Natarajan, H. C. Bajaj and R. J. Tayade, *Water-Energy Nexus*, 2021, **4**, 103–112.
- 185 S. Dehghan, A. J. Jafari, M. FarzadKia, A. Esrafilii and R. R. Kalantary, *Journal of Photochemistry and Photobiology A: Chemistry*, 2019, **375**, 280–292.



[Type here]

- 186 M. Zangiabadi, T. Shamspur, A. Saljooqi and A. Mostafavi, *Applied Organometallic Chemistry*, 2019, 33, e4813.
- 187 S. K. Naynava, B. Lorestani, M. Cheraghi, S. Sobhanardakani and B. Shahmoradi, *Water, Air, & Soil Pollution*, 2024, **235**, 274.
- 188 P. K. Boruah and M. R. Das, *Journal of hazardous materials*, 2020, **385**, 121516.
- 189 S. Akçağlar, *Journal of Chemical Technology & Biotechnology*, 2025, **100**, 138–154.
- 190 P. Nasiripur, M. Zangiabadi and M. H. Baghersad, *Journal of Molecular Structure*, 2021, **1243**, 130875.
- 191 A. Tabasum, I. A. Bhatti, N. Nadeem, M. Zahid, Z. A. Rehan, T. Hussain and A. Jilani, *Water Science and Technology*, 2020, **81**, 178–189.
- 192 A. Tabasum, M. Alghuthaymi, U. Y. Qazi, I. Shahid, Q. Abbas, R. Javaid, N. Nadeem and M. Zahid, *Plants*, 2020, **10**, 6.
- 193 M. A. Khoj, N. S. Awwad, H. A. Ibrahim, A. M. Awad and A. F. Hassan, *Journal of Inorganic and Organometallic Polymers and Materials*, 2024, **34**, 3483–3500.
- 194 M. Dolatabadi, T. Świergosz, C. Wang and S. Ahmadzadeh, *Arabian Journal of Chemistry*, 2023, **16**, 104424.
- 195 F. Soltani-nezhad, A. Saljooqi, T. Shamspur and A. Mostafavi, *Polyhedron*, 2019, **165**, 188–196.
- 196 S. S. Affat, *Univ. Thi-Qar J. Sci.*, 2021, **8**, 130–135.
- 197 H. B. Slama, A. Chenari Bouket, Z. Pourhassan, F. N. Alenezi, A. Silini, H. Cherif-Silini et al., *Appl. Sci.*, 2021, **11**, 6255.
- 198 F. Khan, M. S. Khan, S. Kamal, M. Arshad, S. I. Ahmad and S. A. Nami, *J. Mater. Chem. C*, 2020, **8**, 15940–15955.
- 199 N. A. Al-Rawashdeh, O. Allabadi and M. T. Aljarrah, *ACS Omega*, 2020, **5**, 28046–28055.
- 200 I. F. Waheed, O. Y. T. Al-Janabi and P. J. Foot, *Journal*, 2020, **400**, 125952.
- 201 P. Benjwal, M. Kumar, P. Chamoli and K. K. Kar, *Rsc Advances*, 2015, **5**, 73249–73260.
- 202 S. Banerjee, P. Benjwal, M. K. Singh and K. K. Kar, *Applied surface science*, 2018, **439**, 560–568.
- 203 M. Nadimi, A. Z. Saravani, M. Aroon and A. E. Pirbazari, *Materials Chemistry and Physics*, 2019, **225**, 464–474.
- 204 S. Bibi, A. Ahmad, M. A. R. Anjum, A. Haleem, M. Siddiq, S. S. Shah and A. Al Kahtani, *Journal of Environmental Chemical Engineering*, 2021, **9**, 105580.
- 205 D. P. Ojha, M. K. Joshi and H. J. Kim, *Ceramics International*, 2017, **43**, 1290–1297.
- 206 A. Kumar, L. Rout, L. S. K. Achary, S. K. Mohanty and P. Dash, *New journal of chemistry*, 2017, **41**, 10568–10583.
- 207 A. M. S. Baptisttella, C. M. B. d. Araujo, M. P. da Silva, G. F. O. d. Nascimento, G. R. B. d. Costa, B. F. do Nascimento, M. G. Ghislandi and M. A. d. Motta Sobrinho, *Separation Science and Technology*, 2021, **56**, 425–438.
- 208 S. Sheshmani, B. Falahat and F. R. Nikmaram, *International Journal of Biological Macromolecules*, 2017, **97**, 671–678.
- 209 M. M. Khan, S. F. Adil and A. Al-Mayouf, *J. Saudi Chem. Soc.*, 2015, **19**, 462–464.
- 210 J. Prakash, *Photochem*, 2022, **2**, 651–671.
- 211 T. Imboon, K. Sugio, J. Khumphon, L. Sridawong, V. M. Gowri, K. Yamada, M. Shima and S. Thongmee, *ACS Omega*, 2025, **10**, 34571–34587.
- 212 Denisov, N., Yoo, J., & Schmuki, P. (2019). Effect of different hole scavengers on the photoelectrochemical properties and photocatalytic hydrogen evolution performance of pristine and Pt-decorated TiO2 nanotubes. *Electrochimica Acta*, 319, 61–71.
- 213 Treml, J., & Šmejkal, K. (2016). Flavonoids as potent scavengers of hydroxyl radicals. *Comprehensive reviews in food science and food safety*, 15(4), 720–738.
- 214 Nandi, A., & Chatterjee, I. B. (1987). Scavenging of superoxide radical by ascorbic acid. *Journal of Biosciences*, 11(1), 435–441.
- 215 S. Banerjee, S. C. Pillai, P. Falaras, K. E. O'Shea, J. A. Byrne and D. D. Dionysiou, *J. Phys. Chem. Lett.*, 2014, **5**, 2543–2554.
- 216 S. Wu, H. Hu, Y. Lin, J. Zhang and Y. H. Hu, Visible light photocatalytic degradation of tetracycline over TiO<sub>2</sub>, *Chem. Eng. J.*, 2020, **382**, 122842.
- 217 M. El-Kemary, H. El-Shamy and I. El-Mehasseb, Photocatalytic degradation of ciprofloxacin drug in water using ZnO nanoparticles, *J. Lumin.*, 2010, **130**, 2327–2331.
- 218 S. Yildiz, G. T. Canbaz and H. Mihçioğur, Photocatalytic degradation of oxytetracycline using ZnO catalyst, *Environ. Prog. Sustainable Energy*, 2024, **43**, e14384.
- 219 P. C. H. D. Castillo, V. Castro-Velázquez and V. Rodríguez-González, Adsorption and photocatalytic-conjugated activity of a chitosan-functionalized titanate coating for the removal of the drug clonazepam from drinking water, *Environ. Sci. Pollut. Res.*, 2025, **32**, 10553–10568.
- 220 N. Jallouli, K. Elghniji, H. Trabelsi and M. Ksibi, Photocatalytic degradation of paracetamol on TiO<sub>2</sub> nanoparticles and TiO<sub>2</sub>/cellulosic fiber under UV and sunlight irradiation, *Arab. J. Chem.*, 2017, **10**, S3640–S3645.
- 221 A. O. Iuwole and O. S. Olatunji, Enhanced photocatalytic degradation of naproxen in aqueous matrices using reduced graphene oxide (rGO) decorated binary BSO/g-C<sub>3</sub>N<sub>4</sub> heterojunction nanocomposites, *Chem. Eng. J. Adv.*, 2022, **12**, 100417.
- 222 K. Mitamura, H. Narukawa, T. Mizuguchi and K. Shimada, Degradation of estrogen conjugates using titanium dioxide as a photocatalyst, *Anal. Sci.*, 2004, **20**, 3–4.
- 223 C. F. Carbuloni, J. E. Savoia, J. S. Santos, C. A. Pereira, R. G. Marques, V. A. Ribeiro and A. M. Ferrari, Degradation of metformin in water by TiO<sub>2</sub>-ZrO<sub>2</sub> photocatalysis, *J. Environ. Manage.*, 2020, **262**, 110347.
- 224 I. Uogintė, S. Pleskytė, M. Skapas, S. Stanionytė and G. Lujanienė, Degradation and optimization of microplastic in aqueous solutions with graphene oxide-based nanomaterials, *Int. J. Environ. Sci. Technol.*, 2023, **20**, 9693–9706.
- 225 Q. Wei and M. Zheng, Enhanced photocatalytic degradation of polyethylene microplastics under simulated sunlight using Fe<sub>3</sub>O<sub>4</sub>@TiO<sub>2</sub>/Ag nanocomposite and optimization via response surface methodology, *J. Mater. Sci.: Mater. Electron.*, 2025, **36**, 1675.
- 226 M. Cruz, C. Gomez, C. J. Duran-Valle, L. M. Pastrana-Martinez, J. L. Faria, A. M. Silva and A. Bahamonde, Bare TiO<sub>2</sub> and graphene oxide-TiO<sub>2</sub> photocatalysts on the degradation of selected pesticides and influence of the water matrix, *Appl. Surf. Sci.*, 2017, **416**, 1013–1021.
- 227 M. Hassanpour, H. Safardoust-Hojaghan and M. Salavati-Niasari, Degradation of methylene blue and Rhodamine B as water pollutants via green synthesized Co<sub>3</sub>O<sub>4</sub>/ZnO nanocomposite, *J. Mol. Liq.*, 2017, **229**, 293–299.
- 228 J. T. Adeleke, T. Theivasanthi, M. Thirupathi, M. Swaminathan, T. Akomolafe and A. B. Alabi, Photocatalytic degradation of methylene blue by ZnO/NiFe<sub>2</sub>O<sub>4</sub> nanoparticles, *Appl. Surf. Sci.*, 2018, **455**, 195–200.
- 229 Jamjoum HAA, Umar K, Adnan R, Razali MR and Mohamad Ibrahim MN (2021) Synthesis, Characterization, and Photocatalytic Activities of Graphene Oxide/metal Oxides Nanocomposites: A Review. *Front. Chem.* 9:752276. doi: 10.3389/fchem.2021.752276
- 230 Mandal, S.; Mallapur, S.; Reddy, M.; Singh, J.K.; Lee, D.-E.; Park, T. An Overview on Graphene-Metal Oxide Semiconductor Nanocomposite: A Promising Platform for Visible Light Photocatalytic Activity for the Treatment of

View Article Online

10.1039/D5VA00050F



## ARTICLE

Journal Name

- Various Pollutants in Aqueous Medium. *Molecules* 2020, 25, 5380. <https://doi.org/10.3390/molecules25225380>
- 231 P.M, Visakh & Raneesh, B.. (2020). Metal Oxide Nanocomposites: State-of-the-Art and New Challenges. *10.1002/9781119364726.ch1*.
- 232 Avar, Baris & Panigrahi, Mrutyunjay. (2022). Synthesis and Characterization of Binary Reduced Graphene Oxide/Metal Oxide Nanocomposites. *Physics and Chemistry of Solid State*. 23. 101-112. *10.15330/pcss.23.1.101-112*.
- 233 Yang, Wenshuai & Pan, Mingfei & Huang, Charley & Zhao, Ziqian & Wang, Jianmei & Zeng, Hongbo. (2021). Graphene oxide-based noble-metal nanoparticles composites for environmental application. *Composites Communications*. 24. 100645. *10.1016/j.coco.2021.100645*.
- 234 Soni J, Sethiya A, Sahiba N, Agarwal S. Recent advancements in organic synthesis catalyzed by graphene oxide metal composites as heterogeneous nanocatalysts. *Appl Organomet Chem*. 2021; 35:e6162. <https://doi.org/10.1002/aoc.6162>
- 235 Ameen, Somavia & Fatima, Rida & Ullah, Nadim & Tighezza, Ammar & Ali, Ijaz & Bilal, Uzma & Saleem, Shahroz & Bilal, Abu Summama Sadavi. (2024). Investigation of structural, morphological, thermal, optical, and magnetic properties of graphene-embedded hematite and magnetite nanocomposites. *Optical and Quantum Electronics*. 56. 1-15. *10.1007/s11082-024-07413-4*.
- 236 Ameen, Somavia & Fatima, Rida & Ullah, Nadim & Tighezza, Ammar & Ali, Ijaz & Bilal, Uzma & Saleem, Shahroz & Bilal, Abu Summama Sadavi. (2024). Investigation of structural, morphological, thermal, optical, and magnetic properties of graphene-embedded hematite and magnetite nanocomposites. *Optical and Quantum Electronics*. 56. 1-15. *10.1007/s11082-024-07413-4*.
- 237 Sharma, R., Kumar, H., Yadav, D., Saini, C., Kumari, R., Kumar, G., Kajjam, A. B., Pandit, V., Ayoub, M., Saloni, Deswal, Y., & Sharma, A. K. (2024). Synergistic advancements in nanocomposite design: Harnessing the potential of mixed metal oxide/reduced graphene oxide nanocomposites for multifunctional applications. *Journal of Energy Storage*, 93, 112317. <https://doi.org/10.1016/j.est.2024.112317>
- 238 Ren, G., Han, H., Wang, Y., Liu, S., Zhao, J., Meng, X., & Li, Z. (2021). Recent Advances of Photocatalytic Application in Water Treatment: A Review. *Nanomaterials (Basel, Switzerland)*, 11(7), 1804. <https://doi.org/10.3390/nano11071804>
- 239 Ajala, Oluwaseun & Tijani Oladejo, Jimoh & Mercy Temitope, Bankole & Abdulkareem, A.. (2022). A Critical Review on Graphene Oxide Nanostructured material: Properties, Synthesis, Characterization and Application in Water and Wastewater Treatment. *Environmental Nanotechnology, Monitoring & Management*. 18. 100673. *10.1016/j.enmm.2022.100673*.

View Article Online  
DOI: 10.1039/D6VA00059B

Open Access Article. Published on 14 April 2026. Downloaded on 4/15/2026 12:00:21 AM.  
This article is licensed under a Creative Commons Attribution-NonCommercial 3.0 Unported Licence.



# Towards Sustainable Photocatalytic Degradation of Organic Pollutants through Rational Design of Engineered Magnetically Retrievable Metal Oxide@Graphene Oxide Nanocomposites

Kirti <sup>a</sup>, Anju Srivastava <sup>a\*</sup>, Sriparna Dutta <sup>a\*</sup>, R. K. Sharma <sup>b</sup>, Reena Jain <sup>a</sup>, Prashant Kumar <sup>c</sup>, Ruchi Singh <sup>a</sup>, Priyanka <sup>a</sup>, Vipin Kumar Upadhyay <sup>d</sup>, Geetanshu <sup>a</sup> and Siddharth N Kurur <sup>e</sup>

<sup>a</sup> Department of Chemistry, Hindu College, University of Delhi, Delhi-110007.

<sup>b</sup> Green Chemistry Network Centre, Hindu College, University of Delhi, Delhi-110007.

<sup>c</sup> Department of Chemistry, SRM University Delhi-NCR, Sonapat, Haryana 131029

<sup>d</sup> Department of Chemistry, IIT Kanpur, Kanpur- 208016.

<sup>e</sup> Department of Chemistry, University of Delhi, Delhi-110007.

## Data availability

All data discussed in this review are drawn from previously published sources, which are cited in the reference list.

